AIMS Mathematics, 11(11): 38377–38404.
DOI: 10.3934/math.20261482
Received: 14 September 2026
Revised: 26 October 2026
Accepted: 04 November 2026
Published: 18 November 2026

https://www.aimspress.com/journal/Math

Research article

Fractional conformable derivative photo-electro-magneto-thermoacoustic wave dynamics in a nonlocal semiconductor medium under initial stress

Mashael A. Aljohani[1], A. F. Al-Hazaemh[2,*] and F. S. Bayones[3]

[1] Department of Mathematics and Statistics, College of Science in Yanbu, Taibah University, Yanbu Governorate, Saudi Arabi
[2] Department of Mathematics, Faculty of Science, Sohag University, Sohag, Egypt
[3] Department of Mathematics and Statistics, College of Science, Taif University, P. O. Box 11099, Taif 21944, Saudi Arabia

* **Correspondence:** Email: Ahmadfaruk25@icloud.com; Tel: +962-796-777-036.

Abstract: This work examined the impact of initial stress on the spread of coupled thermo-mechanical waves in a nonlocal semiconductor thermoelastic medium using the fractional conformable derivative model. We presented a novel fractional-order framework for analyzing photo-electro-magneto-thermoacoustic wave propagation in a nonlocal semiconductor medium under the combined effects of the initial stress, electro-magnetic field, and relaxation time. This study investigated the combined effects of the initial stress, nonlocality parameter, magnetic field, and fractional-order derivatives of order α on the photo-thermoacoustic medium, employing the fractional conformable derivative behavior of semiconductors with an internal heat source, with nonlocal effects incorporated into the governing equations. The model incorporates conformable fractional derivatives to capture memory-dependent behavior and employs Eringen's nonlocal elasticity theory to describe microscale interactions. The governing equations were derived by coupling thermoelasticity, carrier transport, electromagnetic fields, and acoustic wave propagation into a unified system. Using Helmholtz decomposition and normal-mode analysis, the problem was reduced to a higher-order characteristic equation that enables analytical solutions. Numerical results demonstrated the significant influence of fractional order, electromagnetic parameters, and initial stress on wave attenuation and dispersion. The proposed model provides a unified framework for investigating the combined effects of fractional-order heat conduction, nonlocality, initial stress, and the magnetic field on the thermo-photoacoustic behavior of semiconductors. The results demonstrate the potential of the proposed model for the design and optimization of high-precision semiconductor devices, optical sensors, thermal management techologies and energy conversion systems operating under complex

physical conditions. The findings provide valuable insights for the design of advanced semiconductor devices and thermal management technologies.

Keywords: fractional thermoacoustics; photo-thermoacoustic waves; nonlocal semiconductor; electromagnetic coupling; initial stress; conformable fractional derivative; normal mode analysis; wave propagation
Mathematics Subject Classification: 35L05, 35Q74, 35R11, 74B05, 74F05, 74J05

Nomenclature

ρ	Density of the medium
$T_\circ$	Absolute temperature
u, w	The displacement components
Π, ψ	Two scalar functions
c_e	The specific heat of the medium
N	The carrier density
T	Temperature distribution
Q	Acoustic pressure
λ, μ	Lame's constants
$\gamma = (3\lambda + 2\mu)\alpha_T$	The volume coefficient of thermal expansion
D_E	The carrier diffusion coefficient
α_T	The linear thermal expansion coefficient
d_n	The coefficients of electronic deformation
$\delta_n = (3\lambda + 2\mu)d_n$	Deformation potential coefficient
E_g	The energy gap
K	Thermal conductivity
t	Time
τ	Lifetime
τ_θ	Phase-lag of the temperature gradient
τ_q	Phase-lag of the heat flux
α	Fractional-order derivatives
$\partial^\alpha/\partial t^\alpha$	Conformable fractional derivative of order α
η	The nonlocal parameter
μ_e	Magnetic permeability
H_o	Magnetic field parameter
σ_{ij}	The stress components
b	Wave number
c	Phase velocity
Γ	Gamma function
P	The initial stress

1. Introduction

The study of thermoelasticity has long been a cornerstone in understanding the coupling between thermal and mechanical fields. Early foundational works established the theoretical framework for irreversible thermodynamics and generalized dynamical thermoelasticity, laying the groundwork for subsequent advances in elastic wave propagation. Semiconductor materials play a crucial role in modern micro- and nano-electronic systems due to their coupled electrical, thermal, and mechanical properties. In particular, the interaction between thermal, elastic, electromagnetic, and carrier transport fields has become a central topic in the modeling of optoelectronic and photo-thermoelastic devices. These materials are frequently subjected to ultrafast laser heating, magnetic fields, and mechanical loading, which induce complex multiphysics wave phenomena that cannot be accurately described using classical thermoelastic theory. The classical theory of thermoelasticity, originally introduced by Biot, is based on Fourier's law of heat conduction, which predicts an infinite speed of thermal propagation. To overcome this limitation, several generalized thermoelastic theories have been developed, including the Lord–Shulman (LS) model, Green–Lindsay (GL) theory, and Green–Naghdi (GN) theory, which introduce thermal relaxation effects and allow finite wave propagation speeds [1–3]. Alshehri and Lotfy [4] regarded the fractional-order Hall-current magneto-photothermal waves in microtemperature hydro-poroelastic semiconductor media subjected to ramp-type heating and variable thermal conductivity. Kamel et al. [5] deemed the photo-thermoacoustic waves propagation flow of excited magneto-nonlocal semiconductors in stability region with varying thermal conductivity. Ahlawat et al. [6] assumed the photo-thermo-acoustic interactions in a fiber-reinforced nonlocal semiconductor medium. Sur [7] thought the photothermoelastic interaction in a two-dimensional semiconductor with nonlocal stress theory. Kaur and Singh [8] examined the plane wave in non-local semiconducting rotating media with Hall effect and three-phase lag fractional order heat transfer. Lotfy et al. [9] investigated the fractional photo-thermoelastic waves of hydrodynamic semiconductors with Hall currents and variable thermal conductivity. Sapa et al. [10] evaluated the excited non-local microelongated semiconductor layer thermal-optical mechanical waves affected by rotational field. Kamel et al. [11] analyzed the novel multi-temperature photoacoustic dynamics in nanoscale hydro-semiconductors under variable thermal conductivity. Biot [12] discussed the thermoelasticity and irreversible thermodynamics. Lord and Shulman [13] the generalized dynamical theory of thermoelasticity. Green and Lindsay [14] addressed the thermoelasticity. White [15] included the generation of elastic waves by transient surface heating. These models have been widely applied in the analysis of wave propagation in elastic and semiconductor media under different physical conditions. Lotfy [16] investigated the photothermal waves for two temperatures with a semiconducting medium under a dual-phase-lag model and hydrostatic initial stress. Youssef et al. [17] considered the photoacoustic wave dynamics in magneto-hydro-semiconductor media with rotation and multi-temperature effects. Youssef et al. [18] formulated the novel model of semiconductor porosity medium according to photo-thermoelasticity excitation with initial stress. Salah et al. [19] addressed the magneto-thermoelastic semiconductor medium with diffusion under the hyperbolic two-temperature photothermal waves. Al-Hazaemh et al. [20] examined the photothermal interactions in micropolar generalized thermoelastic medium subjected to an electromagnetic field. Ismail et al. [21] studied the influence of variable thermal conductivity on thermal-plasma-elastic waves of an excited microelongated semiconductor. Lotfy and Hassan [22] explored the normal mode method for two-temperature generalized thermoelasticity

under the thermal shock problem. Mohamed et al. [23] considered the effect of rotation on plane waves in generalized thermo-microstretch elastic solid with one relaxation time. On the other hand, magneto-thermo-mechanical interactions and electromagnetic coupling effects in elastic and semiconductor structures remain a key area of research due to their importance in modern smart materials and energy systems [24–26]. Wang and Dong [27] investigated the magneto-thermo-dynamic stress and perturbation of magnetic field vector in a non-homogeneous thermo-elastic cylinder. Abd-Alla et al. [28] incorporated the thermal stress in an elastic half-space and its application in partial differential equation. Soliman et al. [29] regarded the highly dispersive gap solitons for conformable fractional model in optical fibers with dispersive reflectivity solutions using the modified extended direct algebraic method. Zhao and Luo [30] viewed the general conformable fractional derivative and its physical interpretation. Eringen [31] investigated the continuum theory of superconductivity. Alarfaj et al. [32] studied the ramp-type heating in a thermoelastic semiconductor medium under coupled plasma and thermal with gravity and initial stress effects. Xuele and Suh [33] considered the generalized thermo-elastodynamics for semiconductor material subject to ultrafast laser heating. Markushev et al. [34] investigated the experimental photoacoustic observation of the photogenerated excess carrier influence on the thermoelastic response of n-type silicon. Fractional thermoelasticity is an advanced generalization of classical thermoelastic theories, incorporating fractional-order derivatives into the equation of energy. Within this framework, heat conduction is extended using fractional derivatives, allowing the model to capture non-Fourier heat transfer phenomena, such as finite-speed thermal wave propagation and dispersive affects. The inclusion of fractional parameters enhances the model's flexibility, improving the description of thermal lag, damping, wave attenuation, and dynamic stability in complex materials. As a result, fractional thermoelasticity provides a more accurate and adaptable approach for analyzing modern engineering systems and advanced material structures, effectively representing behaviors that classical theories cannot fully capture. For further foundational studies on this subject, readers are referred to [35,37]. Ramady et al. [38] discussed the effects of fractional derivative and gravity on wave propagation in micro-elongated thermo-elastic media under the refined dual-phase-lag model. Ramadan et al. [39] regarded the initial stress effects on fractional thermoelastic wave propagation in semiconductor media under three thermoelasticity theories. Zhang [40] evaluated the neural-symbolic exact solutions for camassa–holm equation. Zhao and Zhang [41] investigated the artificial intelligence-enhanced mathematical derivation method: exact solutions of the benjamin–bona–mahony equation. In recent years, researchers have extensively focused on the fractional conformable derivative photo-electro-thermoelastic wave (see for example [42–44], and several references therein).

Despite these extensive studies, most existing works focus on isolated physical effects or simplified media, leaving a gap in understanding the combined influence of initial stress, magnetic fields, nonlocality, and fractional-order effects in semiconductor materials under photothermal excitation. This study addresses this gap by developing a comprehensive model that incorporates all of these factors simultaneously, providing more realistic insights into wave propagation in complex semiconductors. Compared with conventional thermoelastic models, the proposed formulation provides a more comprehensive representation of the coupled thermo-photoacoustic response under complex thermal loading by simultaneously accounting for nonlocality, fractional-order effects, and multiple interacting physical fields, thereby improving the description of wave propagation and coupled thermal-mechanical behavior in semiconductor materials.

The present work employs normal mode analysis to transform the fractional governing equations into a solvable form, enabling a thorough evaluation of temperature, displacement, stress, acoustic pressure, and carrier density. Motivated by this limitation, the present work develops a generalized fractional-order model for photo-electro-magneto-thermoacoustic wave propagation in a nonlocal semiconductor medium under initial stress. The governing equations are formulated by coupling thermoelasticity, Maxwell's electromagnetic equations, carrier density dynamics, and acoustic wave propagation within a unified framework. Eringen's nonlocal elasticity theory is incorporated to capture size-dependent effects, while conformable fractional derivatives are employed to describe memory-dependent thermal and mechanical behavior. The resulting system is solved analytically using Helmholtz decomposition and normal-mode analysis, leading to a characteristic equation governing wave propagation. To back up the analytical findings, numerical computations accompanied by graphical representations are employed to assess how initial stress affects the spatial distributions of displacement, stress components, temperature, and carrier concentration. The computational results show that the frational order has a considerable impact on the semiconductor response, changing wave properties as well as the associated thermoelastic field quantities. The effects of key parameters, including fractional order, magnetic field strength, and initial stress, are investigated numerically to evaluate their influence on displacement, temperature, stress, carrier density, and acoustic pressure fields. The proposed model provides a more comprehensive description of multi-physical interactions in semiconductor materials and may be useful in the design and optimization of microelectronics, photonics, initialisation of fractional order affects, the performance of neural network solutions for fractional differential equations, and sensing devices operating under coupled thermal-electromagnetic environments.

2. Mathematical model and problem description

We consider a homogeneous, isotropic, nonlocal semiconductor occupying the half-space, bounded by the plane surface $z = 0$. The x-axis and y-axislie in the plane of the boundary, while the positive z-axis is directed normally into the semiconductor. The governing equations incorporate the conformable derivative as a local, time-scaled differential operator of order $0 < \alpha \leq 1$. Accordingly, the parameter α modifies the temporal scaling of the governing equations. Unlike nonlocal fractional operators, such as the Caputo and Riemann–Liouville derivatives, the conformable derivative does not intrinsically account for hereditary memory effects. Its use in the present model is motivated by its analytical tractability within the adopted normal-mode formulation, rather than by an assumption that it represents genuine nonlocal temporal memory, and the governing formulation incorporates fractional-order derivatives of order α, where $0 < \alpha \leq 1$. The analysis is conducted within the framework of infinitesimal deformation theory, allowing the linear thermoelastic constitutive relations to be employed. Furthermore, nonlocal elasticity is introduced into the formulation to capture size-dependent effects and the underlying small-scale interactions within the material. The thermoelastic–photoacoustic system is described through four primary field variables: the temperature $T(x, z, t)$, displacement components $u(x, z, t)$ and $w(x, z, t)$, carrier concentration $N(x, z, t)$, and acoustic pressure $Q(x, z, t)$. The magnetic field is prescribed by the vector $\vec{H} = (0, H_0, 0)$, indicating that the field is uniformly oriented along the positive **y**-direction.

The governing equations are formulated within a fractional-order framework by extending established models of fractional photo-thermoelasticity and semiconductor dynamics [19,24,30]. The classical formulations are generalized to incorporate the coupled electromagnetic interactions and the

effects of initial stress. Accordingly, a coupled system of fractional-order equations is obtained to describe the evolution of temperature, displacement, stress, acoustic pressure, and carrier density, thereby accounting for the relevant physical mechanisms of the considered medium.

Following Wang and Dong [27], the governing Maxwell equations for the electrodynamic field are formulated as follows:

$$\vec{J} = curl\,\vec{h}, -\mu_e \frac{\partial \vec{h}}{\partial t} = curl\,\vec{E},\ div\,\vec{h} = 0, div\,\vec{E} = 0, \tag{1}$$

$$\vec{E} = -\mu_e \left(\frac{\partial \vec{u}}{\partial t} \times \vec{H}\right),\ \vec{h} = curl\,(\vec{u} \times \vec{H}), \tag{2}$$

where $\vec{J}$, $\vec{h}$, μ_e, and $\vec{E}$ denote, respectively, the electric current density, the perturbed magnetic-field intensity, the magnetic permeability, and the electric-field intensity.

Accordingly, the preceding relations can be combined to obtain:

$$\vec{E} = -\mu_e \left(-H_\circ \frac{\partial w}{\partial t}, 0, H_\circ \frac{\partial u}{\partial t}\right), \vec{h} = (-H_\circ w, 0, H_\circ u), \vec{j} = -H_\circ \left(\frac{\partial u}{\partial x} + \frac{\partial w}{\partial z}\right). \tag{3}$$

The Lorentz force vector, denoted by $\overrightarrow{F}$, is expressed in the following form:

$$\overrightarrow{F} = \mu_e(\overrightarrow{j} \wedge \overrightarrow{H}). \tag{4}$$

Accordingly, the following expression is obtained:

$$F_x = \mu_e H_0^2 \left(\frac{\partial^2 u}{\partial x^2} + \frac{\partial^2 w}{\partial x \partial z}\right),\ F_z = \mu_e H_0^2 (\frac{\partial^2 u}{\partial x \partial z} + \frac{\partial^2 w}{\partial z^2}. \tag{5}$$

Following the formulation introduced by Zhao and Luo [30], the equations governing the motion of the present model can be expressed as follows:

$$(\lambda + 2\mu + \mu_e \mathrm{H}_\circ^2) \frac{\partial^2 u}{\partial x^2} + \mu \frac{\partial^2 u}{\partial z^2} + (\lambda + \mu + \mu_e \mathrm{H}_\circ^2) \frac{\partial^2 w}{\partial x \partial z} - \gamma \frac{\partial T}{\partial x} - \delta_n \frac{\partial N}{\partial x} - P \frac{\partial\, \omega_{xz}}{\partial z} = [\rho(1 - \eta^2 \nabla^2) + \varepsilon_0 \mu_e^2 H_0^2] \frac{\partial^2 u}{\partial t^2}, \tag{6}$$

$$(\lambda + 2\mu + \mu_e \mathrm{H}_\circ^2) \frac{\partial^2 w}{\partial z^2} + \mu \frac{\partial^2 w}{\partial x^2} + (\lambda + \mu + \mu_e \mathrm{H}_\circ^2) \frac{\partial^2 u}{\partial x \partial z} - \gamma \frac{\partial T}{\partial z} - \delta_n \frac{\partial N}{\partial z} - P \frac{\partial\, \omega_{xz}}{\partial x} = [\rho(1 - \eta^2 \nabla^2) + \varepsilon_0 \mu_e^2 H_0^2] \frac{\partial^2 w}{\partial t^2}. \tag{7}$$

The governing relation describing the carrier-density dynamics in the semiconductor medium can be expressed as follows:

$$\frac{\partial N}{\partial t} = D_E \nabla^2 N - \frac{1}{\tau} N + KT. \tag{8}$$

The governing equation for the propagation of photoacoustic waves can be expressed in the

following form:

$$\nabla^2 P_a - \frac{1}{{c_s}^2}\frac{\partial^2 P_a}{\partial t^2} - \Im\beta\frac{\partial^2 T}{\partial t^2} = 0. \tag{9}$$

Consequently, the governing fractional-order equation for heat conduction.

The resulting fractional-order heat conduction equation is expressed as:

$$\left(1 + \frac{\tau_\theta^\alpha}{\Gamma(1+\alpha)}\frac{\partial^\alpha}{\partial t^\alpha}\right) K\nabla^2 T - \frac{E_g}{\tau}N - \frac{\partial}{\partial t}\left(1 + \frac{\tau_q^\alpha}{\Gamma(1+\alpha)}\frac{\partial^\alpha}{\partial t^\alpha}\right)\left(\gamma T_o\left(\frac{\partial u}{\partial x} + \frac{\partial w}{\partial z}\right) + \rho c_e T\right) = 0, \tag{10}$$

where $\frac{\partial^\alpha}{\partial t^\alpha}$ is the conformable fractional derivative of order $0 \prec \alpha \leq 1$ [29].

$$\Gamma(\alpha + 1) = \alpha\Gamma(\alpha). \tag{11}$$

Definition [30]. Let f be a function such that f: $[a, \infty) \rightarrow$ R. Then, the conformable derivative of a function f is defined as: $D_t^\alpha f(t) = \ell im_{\varepsilon\to 0}\frac{f(t+\varepsilon t^{1-\alpha})-f(t)}{\varepsilon}$. If f is differentiable, then $D_t^\alpha f(t) = t^{1-\alpha}\frac{df(t)}{dt}$, for all $t \geq a$, $\alpha \in (0, 1]$.

The conformable fractional derivative is employed because of its mathematical simplicity and suitability for the analytical treatment of the coupled governing equations. Its derivative-like structure facilitates mathematical manipulation and normal-mode analysis, while the fractional-order parameter α allows investigation of order-dependent temporal scaling and its influence on wave propagation. However, it is a local operator that does not inherently capture long-term memory effects, unlike nonlocal fractional derivatives such as the Caputo and Riemann–Liouville derivatives. Therefore, its main advantage in this study is analytical tractability rather than the direct representation of hereditary behavior. The added discussion clarifies the physical interpretation of the conformable fractional derivative and its role in the coupled thermoelastic and photoacoustic model. It explains how the fractional-order parameter affects the temporal evolution of temperature and may indirectly influence displacement, thermal stress, carrier concentration, and acoustic pressure through thermoelastic coupling. The discussion also highlights the local nature of the conformable derivative, emphasizing that it does not inherently represent long-term memory or produce damping. Finally, it explains that changes in wave propagation and attenuation must be supported by analytical or numerical results, ensuring a physically consistent interpretation of the fractional-order formulation.

By employing Eringen's [31] nonlocal formulation, the nonlocal stress tensor can be expressed as:

$$(1 - \eta^2\nabla^2)\sigma_{xx} = (\lambda + 2\mu + P)\frac{\partial u}{\partial x} + (\lambda + P)\frac{\partial w}{\partial z} - (3\lambda + 2\mu)(\alpha_T T + d_n N), \tag{12}$$

$$(1 - \eta^2\nabla^2)\sigma_{zz} = (\lambda + 2\mu)\frac{\partial w}{\partial z} + \lambda\frac{\partial u}{\partial x} - (3\lambda + 2\mu)(\alpha_T T + d_n N), \tag{13}$$

$$(1 - \eta^2\nabla^2)\sigma_{xz} = \mu\left(\frac{\partial \mathrm{u}}{\partial \mathrm{z}} + \frac{\partial \mathrm{w}}{\partial \mathrm{x}}\right). \tag{14}$$

Here, $c_s = 8430\, m/s$ denotes the acoustic wave speed, while $\beta = 2.56 \times 10^{-6} C^0$ specifies the volumetric coefficient of thermal expansion. The ratio of specific heats, equivalently referred to as the adiabatic index, is given by $\Im = 1.666$. α_T is the coefficient of thermal expansion and d_n denotes

the deformation potential constant. The following derived parameters are introduced for convenience: $\delta_n = (3\lambda + 2\mu)d_n,\ \gamma = (3\lambda + 2\mu)\alpha_T$.

To facilitate the analysis, the governing relations are non-dimensional by introducing appropriate characteristic scales for length, time, temperature, displacement, and stress. This formulation provides a unified framework for evaluating the relative contributions of the various physical parameters.

$$(x', z', u', w', \eta') = \frac{1}{C_T t^*}(x, z, u, w, \eta), N' = \frac{\delta_n N}{\lambda+2\mu}, T' = \frac{\gamma T}{\lambda+2\mu}, P_a' = \frac{P_a}{P_0}, \sigma_{ij}' = \frac{\sigma_{ij}}{\mu}, (t', \tau', \tau_\theta', \tau_q') =$$
$$\frac{1}{t^*}\left(t, \tau, \tau_\theta, \tau_q\right), t^* = \frac{K}{\rho c_e c_T^2}, P' = \frac{P}{\mu},\ K = \rho c_e c_T^2, c_T^2 = \frac{(\lambda+2\mu)}{\rho}, \tag{15}$$

where $\omega_{xz} = \frac{1}{2}\left(\frac{\partial u}{\partial z} - \frac{\partial w}{\partial x}\right),\ \nabla^2 = \left(\frac{\partial^2}{\partial x^2} + \frac{\partial^2}{\partial z^2}\right)$.

Substitution of Eq (15) into Eqs (6)–(10) and (12)–(14) yields the following system of equations, where the prime notation has been omitted for brevity.

$$\frac{\partial^2 u}{\partial x^2} + \varepsilon_1 \frac{\partial^2 u}{\partial z^2} + \varepsilon_2 \frac{\partial^2 w}{\partial x \partial z} - \varepsilon_3 \left(\frac{\partial T}{\partial x} - \frac{\partial N}{\partial x}\right) - \varepsilon_5 \left(\frac{\partial^2 u}{\partial z^2} - \frac{\partial^2 w}{\partial x \partial z}\right) = \varepsilon_8 [\varepsilon_6 \nabla^2 + \varepsilon_7] \frac{\partial^2 u}{\partial t^2}, \tag{16}$$

$$\frac{\partial^2 w}{\partial z^2} + \varepsilon_1 \frac{\partial^2 w}{\partial x^2} + \varepsilon_2 \frac{\partial^2 u}{\partial x \partial z} - \varepsilon_3 \left(\frac{\partial T}{\partial z} - \frac{\partial N}{\partial z}\right) - \varepsilon_5 \left(\frac{\partial^2 u}{\partial x \partial z} - \frac{\partial^2 w}{\partial x^2}\right) = \varepsilon_8 [\varepsilon_6 \nabla^2 + \varepsilon_7] \frac{\partial^2 w}{\partial t^2}, \tag{17}$$

$$\left(1 + \varepsilon_{16} \frac{\partial^\alpha}{\partial t^\alpha}\right) \varepsilon_{17} \nabla^2 \mathrm{T} - \varepsilon_{18} \mathrm{N} - \frac{\partial}{\partial \mathrm{t}} \left(1 + \varepsilon_{19} \frac{\partial^\alpha}{\partial t^\alpha}\right) \left(\varepsilon_{20} \left(\frac{\partial u}{\partial x} + \frac{\partial w}{\partial z}\right) + \varepsilon_{21} T\right) = 0, \tag{18}$$

$$\varepsilon_{11} N \left(\frac{\partial}{\partial t} - \varepsilon_9 \nabla^2 + \varepsilon_{10}\right) - \varepsilon_{12} T = 0, \tag{19}$$

$$\left(\varepsilon_{13} \nabla^2 - \varepsilon_{14} \frac{\partial^2}{\partial t^2}\right) Q\ - \varepsilon_{15} \frac{\partial^2 T}{\partial t^2} = 0, \tag{20}$$

$$(1 - \varepsilon_{22} \nabla^2) \sigma_{xx} = \varepsilon_{23} \frac{\partial u}{\partial x} + \varepsilon_{24} \frac{\partial w}{\partial z} - \varepsilon_{25} (\varepsilon_{26} T + \varepsilon_{27} N), \tag{21}$$

$$(1 - \varepsilon_{22} \nabla^2) \sigma_{zz} = \varepsilon_{23} \frac{\partial w}{\partial z} + \varepsilon_{24} \frac{\partial u}{\partial x} - \varepsilon_{25} (\varepsilon_{26} T + \varepsilon_{27} N), \tag{22}$$

$$(1 - \varepsilon_{22} \nabla^2) \sigma_{xz} = \left(\frac{\partial u}{\partial z} + \frac{\partial w}{\partial x}\right), \tag{23}$$

where

$$\varepsilon_1 = \frac{\mu}{(\lambda + 2\mu + \mu_e \mathrm{H}_\circ^2)}, \varepsilon_2 = \frac{(\lambda + \mu + \mu_e \mathrm{H}_\circ^2)}{(\lambda + 2\mu + \mu_e \mathrm{H}_\circ^2)}, \varepsilon_3 = \frac{(\lambda + 2\mu)}{(\lambda + 2\mu + \mu_e \mathrm{H}_\circ^2)}, \varepsilon_5 = \frac{\mu P}{2(\lambda + 2\mu + \mu_e \mathrm{H}_\circ^2)}, \varepsilon_6$$

$$= \rho - \frac{\eta^2}{c_T^2 t^{*2}}, \qquad \varepsilon_7 = \varepsilon_0 \mu_e^2 \mathrm{H}_0^2,$$

$$\varepsilon_8 = \frac{c_T^2}{(\lambda + 2\mu + \mu_e \mathrm{H}_\circ^2)}, \varepsilon_9 = \frac{D_E}{c_T^2 t^*}, \varepsilon_{10} = \frac{1}{\tau}, \varepsilon_{11} = \frac{1}{\delta_n t^*}, \varepsilon_{12} = \frac{K}{\gamma}, \varepsilon_{13} = \frac{P_\circ}{c_T^2}, \varepsilon_{14} = \frac{P_\circ}{c_s^2}, \varepsilon_{15}$$

$$= \frac{\Im\beta(\lambda + 2\mu)}{\gamma}, \varepsilon_{16} = \frac{\tau_\theta^\alpha}{\Gamma(1+\alpha)}, \varepsilon_{17} = \frac{K(\lambda + 2\mu)}{c_T^2 t^* \gamma}, \varepsilon_{18} = \frac{E_g(\lambda + 2\mu)}{\tau \delta_n}, \varepsilon_{19} = \frac{\tau_q^\alpha}{\Gamma(1+\alpha)}, \varepsilon_{20}$$

$$= \gamma T_0, \varepsilon_{21} = \frac{\rho c_e(\lambda + 2\mu)}{\gamma}, \varepsilon_{22} = \frac{\eta^2}{c_T^2 t^{*2}}, \varepsilon_{23} = \frac{(\lambda + 2\mu + \mu P)}{\mu}, \varepsilon_{24} = \frac{(\lambda + \mu P)}{\mu}, \varepsilon_{25}$$

$$= \frac{(3\lambda + 2\mu)}{\mu}, \varepsilon_{26} = \frac{\alpha_t(\lambda + 2\mu)}{\gamma}, \qquad \varepsilon_{27} = \frac{d_n(\lambda + 2\mu)}{\delta_n}.$$

3. Solution of the problem

Following the Helmholtz decomposition, the displacement field is represented in terms of an irrotational scalar potential $\emptyset$ and a solenoidal vector potential φ as follows:

$$u = \frac{\partial \emptyset}{\partial x} - \frac{\partial \varphi}{\partial z} \text{ and } w = \frac{\partial \emptyset}{\partial z} + \frac{\partial \varphi}{\partial x}. \tag{24}$$

Substituting the representation defined by Eq (24) into Eqs (16)–(18) leads to the corresponding transformed governing system, in which the resulting equations are fully decoupled:

$$\frac{\partial^2 \emptyset}{\partial x^2} - \frac{\partial^2 \varphi}{\partial x \partial z} + \varepsilon_1 \frac{\partial^2 \emptyset}{\partial z^2} + \varepsilon_2 \left(\frac{\partial^2 \emptyset}{\partial z^2} + \frac{\partial^2 \varphi}{\partial x \partial z}\right) - \varepsilon_3 (T + N) + \varepsilon_5 \frac{\partial^2 \varphi}{\partial x \partial z} = \gamma_1 \frac{\partial^3 \emptyset}{\partial x \partial t^2} + \gamma_2 \frac{\partial^2 \emptyset}{\partial t^2}, \tag{25}$$

$$\frac{\partial^2 \varphi}{\partial z^2} + \varepsilon_1 \left(\frac{\partial^2 \emptyset}{\partial x \partial z} + \frac{\partial^2 \varphi}{\partial x^2}\right) + \varepsilon_2 \left(\frac{\partial^2 \emptyset}{\partial x \partial z} + \frac{\partial^2 \varphi}{\partial z^2}\right) - \varepsilon_5 \left(\frac{\partial^2 \varphi}{\partial z^2} - \frac{\partial^2 \varphi}{\partial x^2}\right) = \gamma_1 \frac{\partial^3 \varphi}{\partial x \partial t^2} + \gamma_2 \frac{\partial^2 \varphi}{\partial t^2}, \tag{26}$$

$$\varepsilon_{17} \nabla^2 \mathrm{T} \left(1 + \varepsilon_{16} t^{1-\alpha} \frac{d}{dt}\right) - \varepsilon_{18} \mathrm{N} - \frac{\partial}{\partial \mathrm{t}} \left(1 + \varepsilon_{19} t^{1-\alpha} \frac{d}{dt}\right) \left(\varepsilon_{20} \left(\frac{\partial^2 \emptyset}{\partial x^2} - \frac{\partial^2 \varphi}{\partial z^2} + \frac{\partial^2 \emptyset}{\partial z^2} + \frac{\partial^2 \varphi}{\partial x \partial z}\right) + \varepsilon_{21} T\right) = 0, \tag{27}$$

where $\gamma_1 = \varepsilon_8 \varepsilon_6,\ \gamma_2 = \varepsilon_8 \varepsilon_7$.

4. Derivation of the analytical solution framework

The wave-field variables are subsequently transformed into normal mode form, thereby facilitating the analytical treatment of the governing equations and the characterization of wave propagation [35]:

$$(\emptyset, \varphi, T, N, P_a, \sigma_{ij})(x, z, t) = (\emptyset^*, \varphi^*, T^*, N^*, P_a^*, \sigma_{ij}^*)(x) e^{ib\left(\frac{ct^\alpha}{\alpha} - z\right)}. \tag{28}$$

The conformable fractional derivative is defined as $D_t^{\alpha} f(t) = t^{1-\alpha} \frac{df(t)}{dt}$, where $\alpha \in (0, 1]$. Thus, the stretched-time representation converts conformable time derivatives into constant algebraic multipliers, while ordinary time derivatives are evaluated separately. Here, c represents the phase velocity, $i^2 = -1$ is the imaginary unit, and b denotes the wave number with the z-direction. By applying the prescribed normal-mode representation together with the defining property of the conformable fractional derivative, both the fractional- and integer-order time derivatives can be expressed in algebraic form. Inserting the resulting expressions into Eqs (19), (20), and (25)–(27), and subsequently removing the common exponential factor leads to:

$$(D^2 - \delta_1 D - \beta_1)\emptyset^*(\boldsymbol{x}) + (\beta_2 D - \beta_3)\varphi^*(x) - \varepsilon_3\big(T^*(x) - N^*(x)\big) = 0, \tag{29}$$

$$(\beta_4 D)\emptyset^*(\boldsymbol{x}) + (\beta_5 D^2 - \delta_1 D - \beta_6)\varphi^*(x) = 0, \tag{30}$$

$$(\beta_7 D^2 + \beta_8)N^*(x) - \varepsilon_{12} T^*(x) = 0, \tag{31}$$

$$(\varepsilon_{13} D^2 - \beta_9)P_a^*(x) + \beta_{10} T^*(x) = 0, \tag{32}$$

$$(\beta_{11}(D^2 - b^2))P_a^* + \big(\beta_{11}(b^2 + ibD)\big)\varphi^*(x) - \varepsilon_{18} N^*(x) + (\beta_{12}(D^2 - b^2) - \beta_{13})T^*(x) = 0. \tag{33}$$

Combining Eqs (29)–(33) and eliminating the relevant field variables yields a homogeneous differential equation of order ten:

$$[D^{10} - S_{11}D^8 - S_{12}D^6 - S_{13}D^4 - S_{14}D^2 + S_{15}]\{Q^*, \varphi^*, T^*, N^*, P_a^*\} = 0. \tag{34}$$

Applying the proposed formulation to Eq (34) yields the following characteristic equation:

$$\lambda^{10} - S_{11}\lambda^8 - S_{12}\lambda^6 - S_{13}\lambda^4 - S_{14}\lambda^2 + S_{15} = 0. \tag{35}$$

Appendix A presents the definitions of the constants $S_{11}, S_{12}, \ldots, S_{15}$. Solving Eq (35) yields the following expressions:

$$T^*(x) = \sum_{k=1}^{5} A_k e^{-\lambda_k x}, \tag{36}$$

$$N^*(x) = \sum_{k=1}^{5} A_k V_{k+10} e^{-\lambda_k x}, \tag{37}$$

$$P_a^*(x) = \sum_{k=1}^{5} A_k V_{k+15} e^{-\lambda_k x}, \tag{38}$$

$$\emptyset^*(x) = \sum_{k=1}^{5} A_k V_{k+20} e^{-\lambda_k x}, \tag{39}$$

$$\varphi^*(x) = \sum_{k=1}^{5} A_k V_{k+25} e^{-\lambda_k x}, \tag{40}$$

$$u^* = \sum_{k=1}^{5} A_k e^{-\lambda_k x}(-\lambda_k V_{k+20} + ibV_{k+25}), \tag{41}$$

$$w^* = \sum_{k=1}^{5} A_k e^{-\lambda_k x}(ibV_{k+20} - \lambda_k V_{k+25}), \tag{42}$$

$$\sigma_{xx}^* = \sum_{k=1}^{5} \frac{A_k e^{-\lambda_k x}}{(1 - \varepsilon_{22}\lambda_k^2 + \varepsilon_{22} b^2)}(-\varepsilon_{23}\lambda_k(-\lambda_k V_{k+20} + ibV_{k+25}) - ib\varepsilon_{24}(ibV_{k+20} - \lambda_k V_{k+25}) - \varepsilon_{25}\varepsilon_{26} - \varepsilon_{26}\varepsilon_{27} V_{k+10}), \tag{43}$$

$$\sigma_{xz}^* = \sum_{k=1}^{5} \frac{A_k e^{-\lambda_k x}}{(1 - \varepsilon_{22}\lambda_k^2 + \varepsilon_{22} b^2)}(ib(-\lambda_k V_{k+20} + ibV_{k+25}) - \lambda_k(ibV_{k+20} - \lambda_k V_{k+25})), \tag{44}$$

where

$$V_{1k} = \frac{\varepsilon_{12}}{\beta_7\lambda_k^2 + \beta_8}, V_{1(k+5)} = \frac{\beta_{10}}{\beta_9 - \varepsilon_{13}\lambda_k^2}, V_{2k}$$

$$= \frac{-(\frac{(\beta_{11}b^2 - \beta_{11}ib\lambda_k)(\varepsilon_3 + \varepsilon_3 V_{k+10})}{(-\beta_2\lambda_k - \beta_3)})}{(\beta_{11}\lambda_k^2 - b^2\beta_{11} + \frac{(\beta_{11}b^2 - \beta_{11}ib\lambda_k)(-\lambda_k^2 + \delta_k\lambda_k - \beta_1)}{-\beta_2\lambda_k - \beta_3})}, V_{(k+25)}$$

$$= \frac{-\left(\lambda_k^2 + \delta_k\lambda_k - \beta_1\right)(V_{20+k}) + (\varepsilon_3 + \varepsilon_3 V_{10+k})}{(-\beta_2\lambda_k - \beta_3)}.$$

5. Boundary conditions

To determine the unknown coefficients $A_1, \ldots, A_5$ the prescribed boundary conditions are applied at the surface $\boldsymbol{x} = \mathbf{0}$. Within the framework of the normal-mode formulation, these conditions can be expressed in the following form:

$$\sigma_{xx}{}^* = 0, \sigma_{xz}{}^* = 0, T^* = Q_o, P_a^* = 0, N^* = R_N. \tag{45}$$

The boundary conditions are imposed at $z = 0$. The semiconductor is subjected to prescribed thermal, photoacoustic, and carrier-density excitations at the boundary, together with the specified mechanical traction condition. These boundary data are incorporated into the linear algebraic system used to determine the unknown coefficients of the analytical solution. The adopted boundary constraints comprise a vanishing traction condition, a prescribed thermal excitation, together with prescribed photoacoustic pressure and carrier-density conditions at the surface. The boundary constraints lead to a homogeneous linear system governing the unknown coefficients $\mathrm{A}_1, \ldots, \mathrm{A}_5$. These coefficients are evaluated symbolically using Mathematica software, providing the basis for the subsequent derivation of the field quantities.

6. Validation of the model

To validate the present formulation, a special case is first considered by neglecting the magnetic field effect $(H_0 = 0)$. Under these assumptions, the governing equations reduce exactly to those presented by Ramadan et al. [39]. An excellent agreement is observed for all physical quantities, confirming the correctness and reliability of the developed mathematical formulation and the numerical procedure. Moreover, the amplitudes of all physical quantities increase with increasing time, while the agreement between the present and published results becomes more pronounced with increasing distance. As a second limiting case, when the plasma wave (which is illustrated by carrier density $N(x, z, t)$ is ignored, the thermoelasticity theory is obtained and the results agree with Abd-Alla et al. [28] $(N = 0, H_0 = 0, P = 0, \alpha = 1)$. To validate the present formulation, a special case is first considered by neglecting the magnetic field and initial stress effect $(P = 0)$. Under these assumptions, the governing equations reduce exactly to those presented by Kamel et al. [5].

This qualitative agreement further confirms the validity, consistency, and applicability of the proposed model.

7. Numerical analysis and physical interpretation

Numerical simulations are performed to investigate the effects of electromagnetic field intensity, initial stress, and fractional-order parameters on the fractional photo-thermoacoustic response of nonlocal semiconductor media. Germanium (Ge) is selected as the representative material, with all simulations based on experimentally established material properties. The resulting distributions of the primary field variables, including displacement, temperature, carrier density, acoustic pressure, and stress, are computed using Mathematica software. These results provide a detailed assessment of both the individual and coupled influences of the governing parameters on wave propagation characteristics and stability within the medium.

Table 1. Parameters for material.

Parameter	Symbol	Value	Unit	Parameter	Symbol	Value	Unit
Lame's constant	λ	4.8×10^{10}	$N.m^{-2}$	Coefficient of carrier diffusion	D_E	0.5×10^{-2}	$m^2.s^{-1}$
Lame's constant	μ	5.3×10^{10}	$N.m^{-2}$	Coefficient of electronic deformation	d_n	-6×10^{-31}	$m^2.s^{-1}$
Density	ρ	5300	$kg.m^{-3}$	Carrier concentration	N_0	2×10^{13}	cm^{-3}
Absolute temperature	T_0	723	K	Energy gap	E_g	0.72	eV
Thermal conductivity	K	60	$W.m^{-1}K^{-1}$	Thermoelastic coupling	$\tilde{s}$	2	$W.m^{-1}K^{-1}$
Specific heat	C_e	310	$J.Kg^{-1}.K^{-1}$	Magnetic permeability	ε_0	$4\pi \times 10^{-7}$	$H \cdot m^{-1}$
Thermal expansion	α_T	5.8×10^{-6}	K^{-1}	Heat source	Q_0	10^3	$W \cdot m^{-2}$
Phase-lag of the heat flux	τ_q	0.2	Sec(s)	Phase-lag of the temperature gradient	τ_θ	0.1	Sec(s)
Lifetime of photo-generated carriers	$\tau = 1.4 \times 10^{-6}$		$Sec(s)$	Nonlocal parameter	η	2×10^{-1}	m^2

In this paper, numerical simulations are conducted at a fixed non-dimensional time $(t = 0.4)$, angular frequency $\omega = 0.1$, wave number $b = 0.3$, fractional order $\alpha = 0.3$, initial stress $P = 1.2$, electric permittivity $\varepsilon_0 = 0.04$, magnetic field $H_0 = 1.3 \times 10^5$, and surface position $z = 0.5$ to examine the spatial distribution of displacement components u, w, carrier density N, temperature T, stresses tensor σ_{xx} and σ_{xz}, acoustic pressure P_a, and along the x-axis. To enhance convenience, we have organized the graphs into three distinct categories. In the first set of groups, Figures 1–7 illustrate how the various wave profiles are influenced by the time t, magnetic field H_0, wave number b,

angular frequency ω, fractional order α, phase-lag of the temperature gradient τ_θ, electric permittivity ε_0, and initial stress P utilizing three distinct values of magnetic field, rotation, and laser pulse time on the physical quantities.

Figure 1 depicts the spatial distributions of displacement components u, w, temperature T, normal stress σ_{xx}, shear stress σ_{xz}, carrier density N, and acoustic pressure P_a along the x-axis at $(t = 0.4)$, $(t = 0.6)$, and $(t = 0.8)$. As the magnetic field intensity increases, the displacement components, temperature, normal stress, shear stress, carrier density, and decrease acoustic pressure, while there is oscillatory behavior in the whole range axial x, which tends to decrease. This behavior can be explained by the way time interacts with the coupled thermoelastic and carrier dynamics in the semiconductor. An increase in time enhances the body force acting along the material, promoting deformation and generating higher displacements, which in turn elevates the local temperature through enhanced thermoelastic coupling. The increase in displacement also contributes to higher shear stresses as the material layers slide relative to each other under time. Conversely, the normal stress along the primary direction decreases because the material tends to expand more freely under the influence of time, reducing compressive or tensile stresses in that direction. The carrier density diminishes slightly as the time modifies the distribution of charge carriers, effectively spreading them over a larger volume and reducing local concentration. Similarly, acoustic pressure decreases because the time effect counteracts the pressure waves generated by thermal and mechanical perturbations, attenuating their amplitude. Overall, time introduces a direction-dependent modulation in the material response, enhancing certain field components while suppressing others, reflecting the complex interplay between mechanical, thermal, and carrier phenomena in nonlocal semiconductors. The obtained trends are in agreement with previous investigations on time-induced thermoelastic responses in media [13,14]. Compared with these studies, the present model shows that the combined effects of time, nonlocality, and fractional-order heat conduction produce a more pronounced isotropic response, leading to different variations in the thermal and mechanical fields.

Figure 2 shows the spatial distributions of displacement components u, w, temperature T, normal stress σ_{xx}, shear stress σ_{xz}, carrier density N, and acoustic pressure P_a along the x-axisat $(H_0 = 1.3 \times 10^5)$, $(H_0 = 2.4 \times 10^5)$, and $(H_0 = 3.2 \times 10^5)$. As the magnetic field intensity increases, the physical quantities displacement components, temperature, shear stress, carrier density, and acoustic pressure decrease, while normal stress is oscillatory in the whole range axial x. This behavior can be attributed to the influence of the Lorentz force on the motion of charge carriers within the semiconductor. The magnetic field modifies the trajectories of electrons and holes, enhancing carrier accumulation in certain regions, which directly increases the local carrier density. The augmented carrier density leads to greater energy dissipation through Joule heating, resulting in a rise in temperature along the material. The elevated temperature, in turn, drives stronger thermoelastic forces, amplifying the mechanical displacement and generating higher acoustic pressure. Consequently, the induced temperature gradients and deformations produce larger elastic stresses in the semiconductor. Overall, the increase in magnetic field intensity strengthens the coupling between magnetic, thermal, and mechanical fields, enhancing the overall energy density and wave amplitudes. This effect is particularly significant for device design, as high magnetic fields can elevate local stresses and temperatures, potentially impacting the reliability and performance of rotating semiconductor devices. This behavior is consistent with previous studies on magneto-thermoelastic semiconductors [7,12,15,18], which reported that magnetic fields enhance carrier transport and thermoelastic coupling through the Lorentz force. However, the present model further demonstrates that incorporating fractional-order derivatives together with nonlocality intensifies the coupling between the thermal, mechanical, and carrier fields, providing a more comprehensive description of

the semiconductor response.

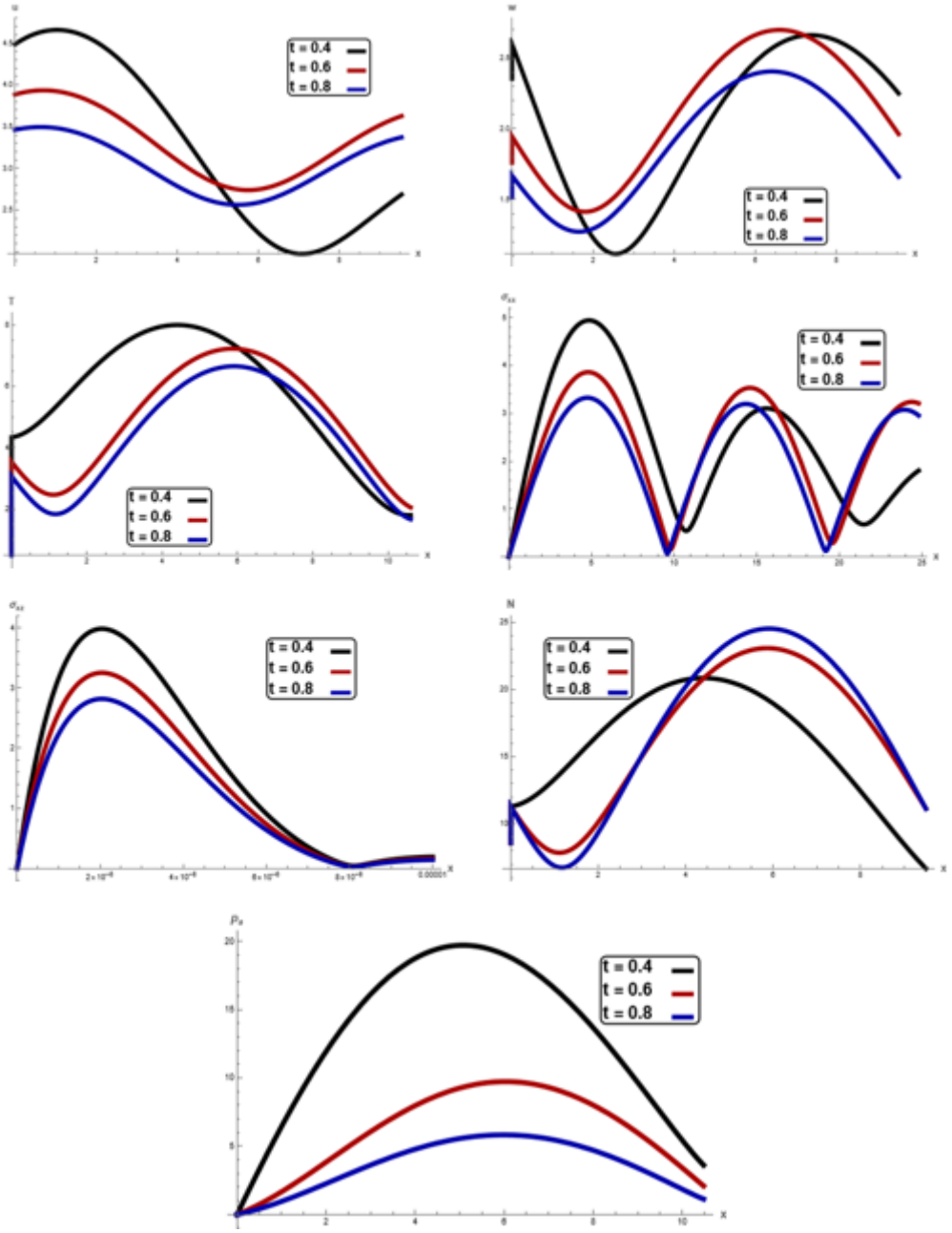


Figure 1. Temporal evolution of the physical fields at different time $(\mathbf{t})$ instants.

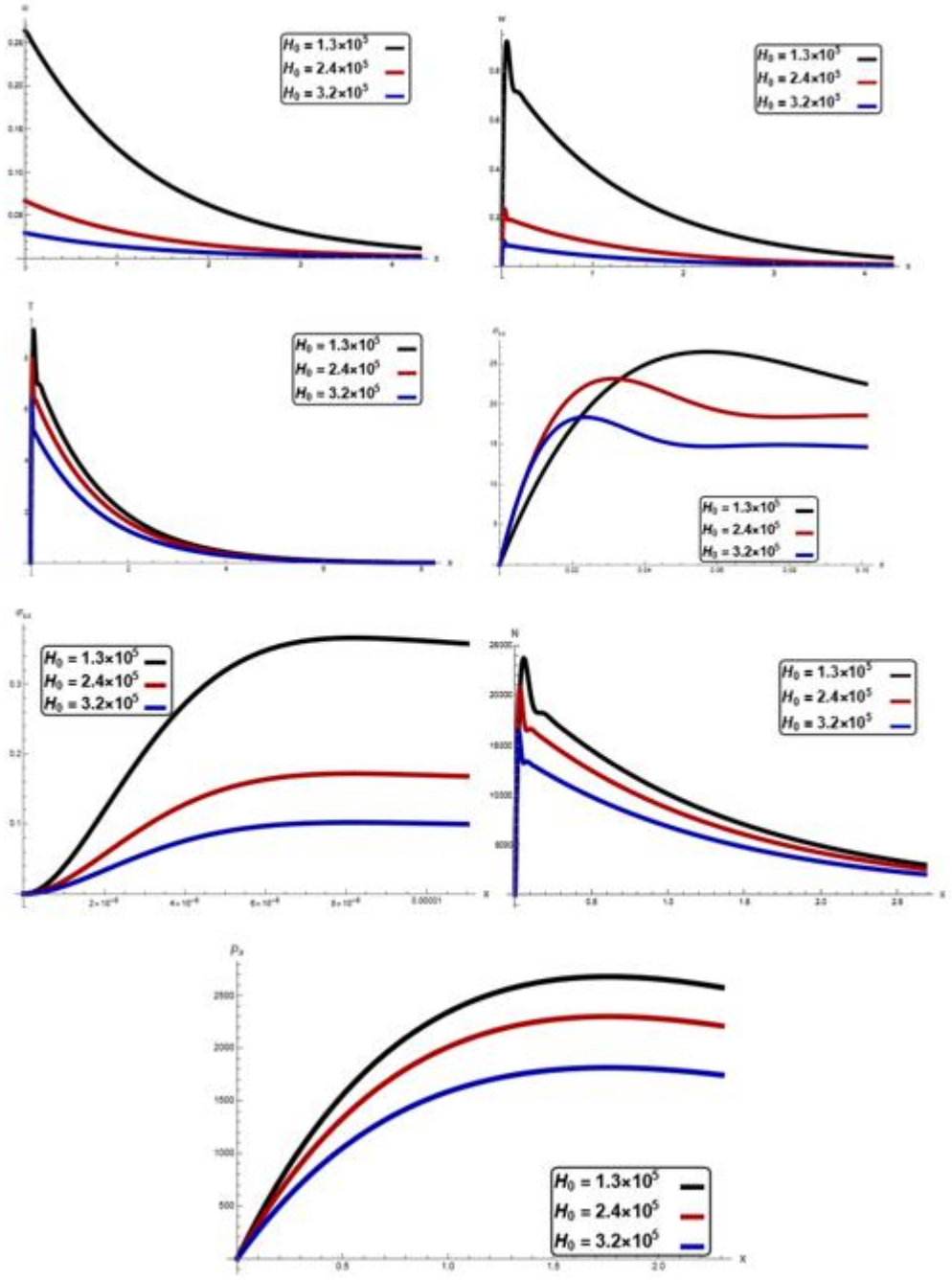


Figure 2. Effect of the magnetic field $(\mathbf{H_0})$ on the evolution of the physical fields.

Figure 3 presents the spatial distributions of displacement components u, w, temperature T, normal stress σ_{xx}, shear stress σ_{xz}, carrier density N, and acoustic pressure P_a along the x-axis at $(\alpha = 0.25)$, $(\alpha = 0.5)$, and $(\alpha = 0.75)$. As α increases, displacement components, temperature, normal stress, shear stress, carrier density, and acoustic pressure show a pronounced rise, whereas it is oscillatory in the whole range of axial x. This behavior can be explained by the fractional-order dynamics, which modulate the rate of energy propagation and dissipation in the semiconductor. Higher values of α correspond to a system closer to classical behavior, where energy transport is more efficient and less dissipative. Consequently, the increase in α allows more thermal and carrier energy to a cumulate in the material, raising the local temperature and carrier density, which in turn enhances acoustic pressure and normal stress. Meanwhile, the improved energy confinement restricts lateral

deformations, resulting in smaller displacements and reduced shear stresses. Overall, the fractional order controls the balance between energy propagation and damping, with higher α promoting stronger thermo-mechanical responses while limiting material deformation, highlighting its critical role in tuning the dynamic behavior of rotating nonlocal semiconductors. The observed behavior agrees with previous findings on fractional thermoelastic systems [5,6,19,21], where increasing the fractional-order parameter reduces memory effects and drives the response toward the classical model. The present study further extends these results by incorporating nonlocality, initial stress, and magnetic field into a unified semiconductor model, allowing their combined influence on the coupled thermo-photoacoustic response to be examined.

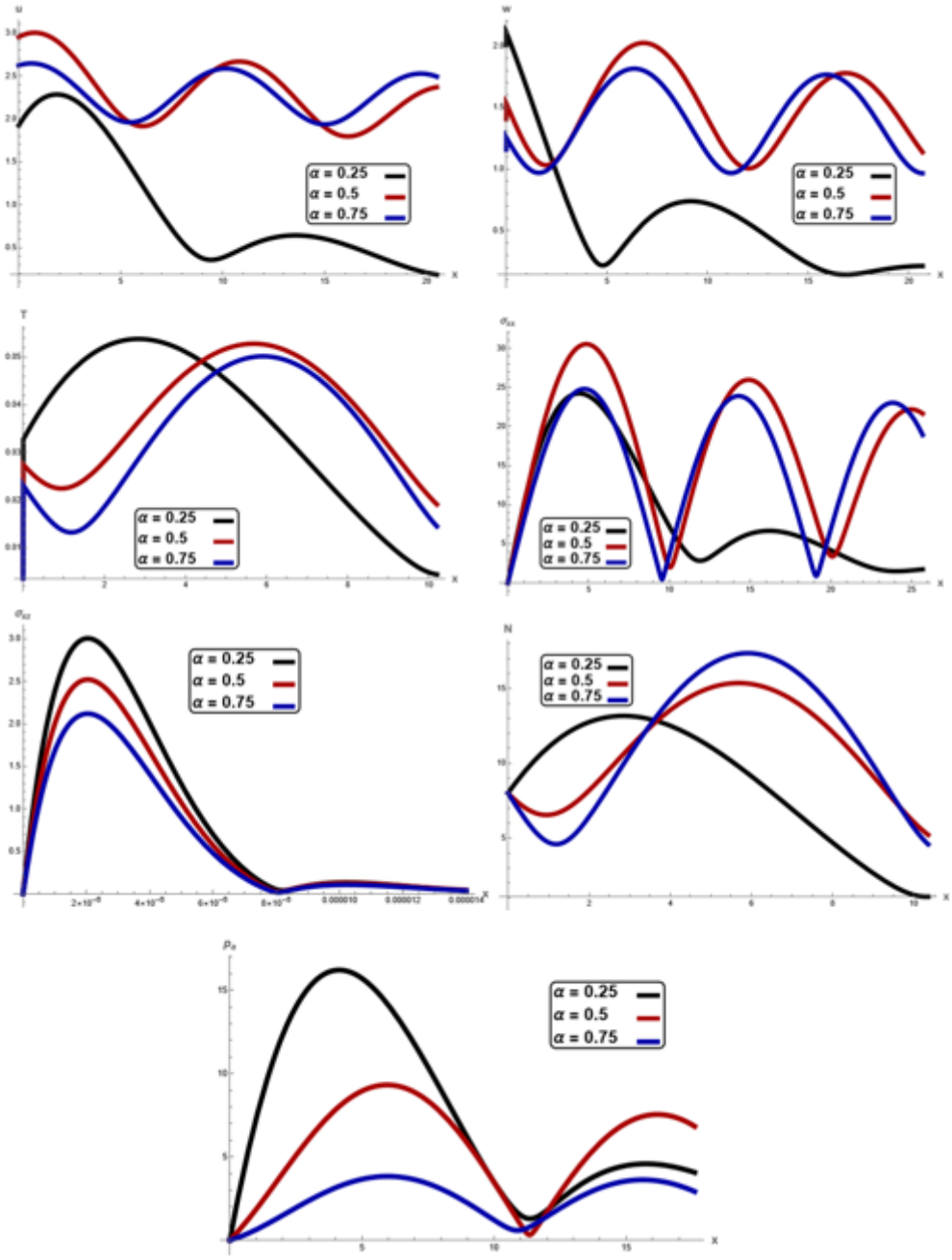


Figure 3. Influence of the fractional order (α) on the physical fields.

Figure 4 depicts the spatial distributions of displacement components u, w, temperature T, normal stress σ_{xx}, shear stress σ_{xz}, carrier density N, and acoustic pressure P_a along the x-axis at $(P = 1.2)$, $(P = 1.7)$, and $(P = 2.3)$. As the initial stress intensity increases, a distinct pattern emerges: displacement components, normal stress, carrier density, and acoustic pressure are oscillatory in the whole range axial x, while shear stress decreases with an increase of initial stress and temperature increases with an increase of initial stress. This behavior can be explained by the way initial stress interacts with the coupled thermoelastic and carrier dynamics in the semiconductor. An increase in initial stress enhances the body force acting along the material, promoting deformation and generating higher displacements, which in turn elevates the local temperature through enhanced thermoelastic coupling. The increase in displacement also contributes to higher shear stresses as the material layers slide relative to each other under initial stress loading. Conversely, the normal stress along the primary direction decreases because the material tends to expand more freely under the influence of initial stress, reducing compressive or tensile stresses in that direction. The carrier density diminishes slightly as the initial stress modifies the distribution of charge carriers, effectively spreading them over a larger volume and reducing local concentration. Similarly, acoustic pressure decreases because the initial stress effect counteracts the pressure waves generated by thermal and mechanical perturbations, attenuating their amplitude. Overall, gravity introduces a direction-dependent modulation in the material response, enhancing certain field components while suppressing others, reflecting the complex interplay between mechanical, thermal, and carrier phenomena in a semiconductors medium. The obtained trends are in agreement with previous investigations on initial stress-induced thermoelastic responses in media [13,14]. Compared with these studies, the present model shows that the combined effects of initial stress and fractional-order heat conduction produce a more pronounced anisotropic response, leading to different variations in the thermal and mechanical fields.

Figure 5 The given plot illustrates the variation of the physical quantities: displacement components, temperature, normal stress, shear stress, carrier density, and acoustic pressure along x-axis at $(b = 0.5)$, $(b = 0.7)$, and $(b = 0.9)$ as a function of horizontal distance for different values of wave number b, as indicated in the legend. However, if the wave number increases, there is a clear trend of decreasing magnitude in the physical quantities, while the u, N increase with an increase of the wave number. This highlights the impactful relationship between the wave number and the resulting amplitude of the physical quantities. This clearly reveals that the $\sigma_{xx}, \sigma_{xz}, m_{xy}, N, w$ increase with an increase of the axial x, while $u, \emptyset_2, \theta$ decrease with increasing of axial x. The $u, w, \theta,\ \sigma_{xx}, \sigma_{xz}, m_{xy}, N, \emptyset_2$ reveal how uncertainties in thermal and mechanical excitation influence stress wave propagation, which is particularly important in high-precision applications. We notice that the physical quantities satisfied the boundary conditions. This type of analysis helps identify regions where the system exhibits high responsiveness, as well as areas where it remains relatively unaffected by parameter changes. It is also observed that as the value of increases, the magnitude of $u, w, \theta,$ $\sigma_{xx}, \sigma_{xz}, m_{xy}, N$ and $\emptyset_2$ increase rapidly and beyond a certain point in the region, which agrees with the GreenNaghdi theory of thermoelasticity. The one common observation in the physical quantities is the higher the value of b, the higher is the amplitude. These results are consistent with previous studies on rotating nonlocal semiconductor models (Al-Hazaemh et al. [27]), where the wave number modifies the mechanical and thermal responses. In addition, the present analysis demonstrates that the wave number influences the coupled thermoelastic and carrier-field responses of the semiconductor medium. Physically, variations in the wave number modify the spatial distribution of the physical fields and may affect thermal localization near the boundary surface. The carrier-density distribution exhibits a positive value near the surface and gradually decreases with distance into the

semiconductor, consistent with the spatial attenuation of photo-generated carriers reported in experimental studies [33,34]. This behavior reflects the transport and recombination of excess charge carriers generated by optical excitation. As the carrier density approaches zero, the excess-carrier concentration diminishes with increasing distance from the surface.

Overall, the results demonstrate that the magnetic field, initial stress, time, fractional-order parameter, and wave number influence the thermo-photoacoustic response of the semiconductor medium. These findings highlight the role of nonlocal elasticity and fractional-order derivatives in describing the coupled thermal, mechanical, and carrier-field behavior of semiconductor materials.

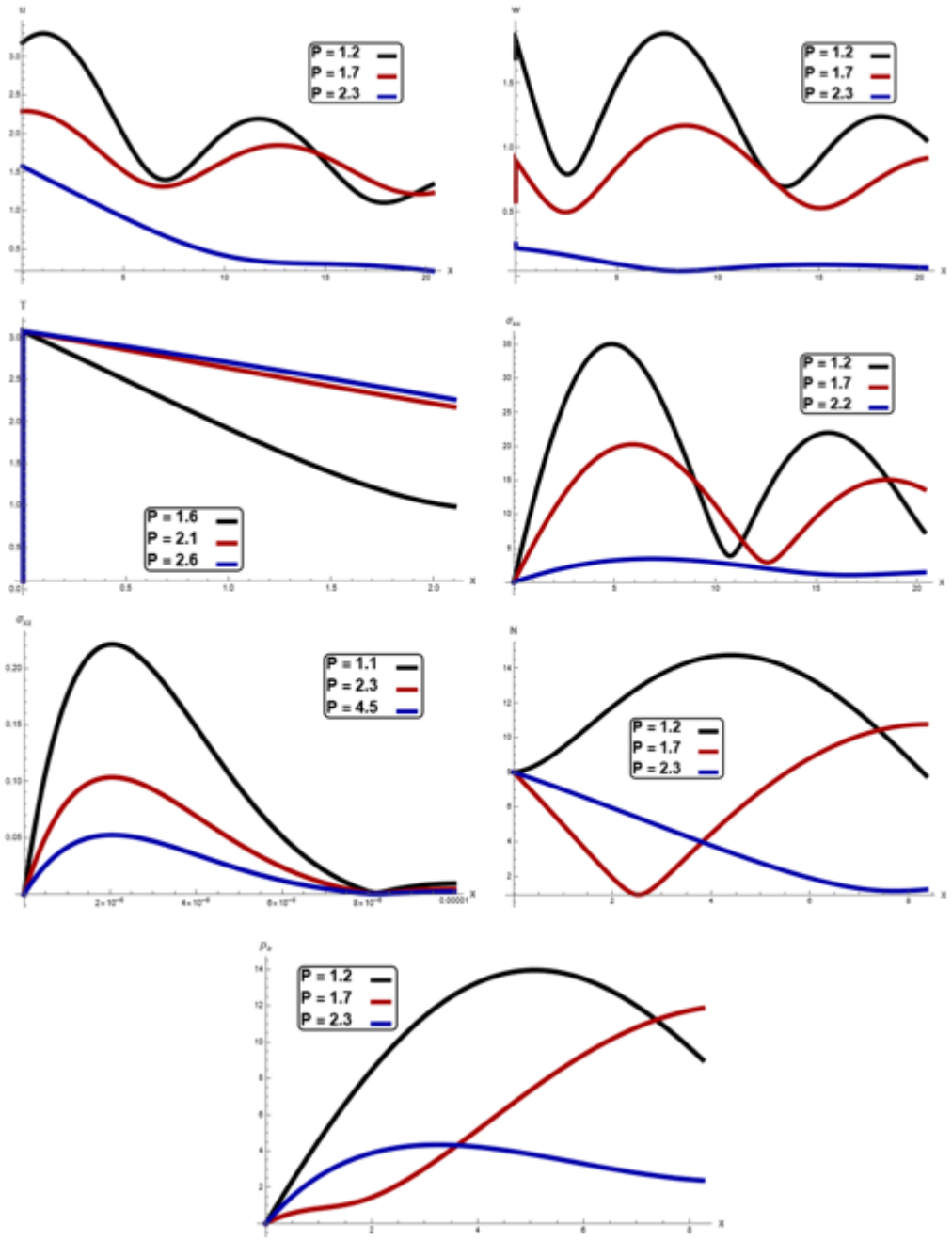


Figure 4. Influence of initial stress (**P**) on the temporal evolution of the physical fields.

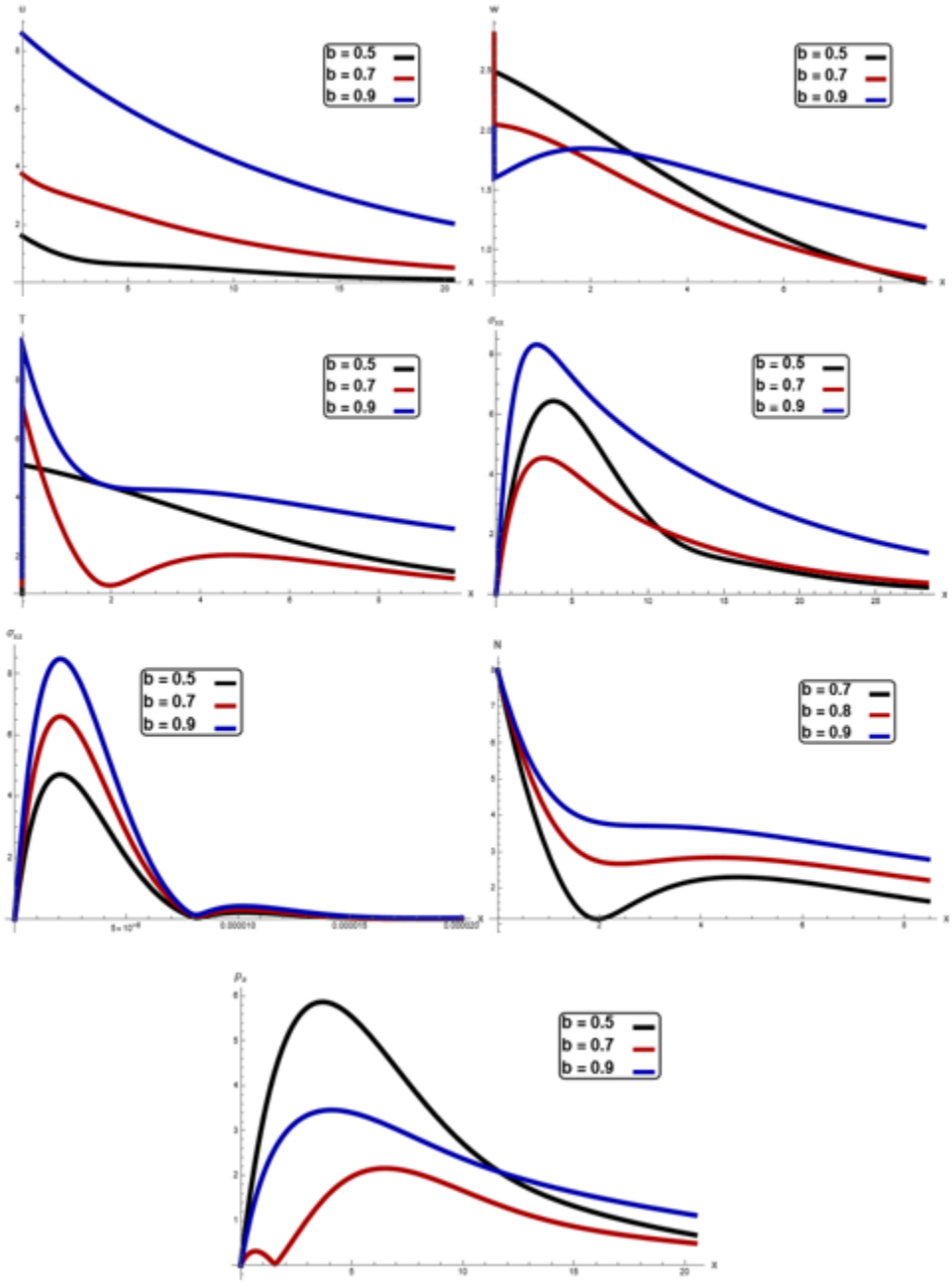


Figure 5. Effect of wave number $(\mathbf{b})$ on the evolution of the physical fields.

Figure 6 illustrates the spatial distributions of the displacement components, temperature, normal stress, shear stress, carrier density, and acoustic pressure along the x-axis for different values of the electric-field parameter at $(\varepsilon_0 = 1.4 \times 10^5)$, $(\varepsilon_0 = 2.5 \times 10^5)$, and $(\varepsilon_0 = 3.6 \times 10^5)$. The numerical results demonstrate that variations in the electric field modify the amplitudes and spatial profiles of the coupled physical fields, with some quantities exhibiting pronounced peaks, oscillatory behavior, or gradual attenuation along the semiconductor medium. These changes reflect the influence of electromagnetic coupling on the interaction between mechanical deformation, thermal transport, and charge-carrier dynamics.

Physically, the electric field affects the motion and redistribution of charge carriers, thereby modifying the carrier-density distribution and its coupling with the thermal and mechanical fields.

Changes in carrier transport influence the redistribution of energy within the medium, which can subsequently alter the temperature field and the associated thermoelastic deformation. The resulting changes in displacement and temperature gradients are reflected in the normal and shear stresses, while the acoustic pressure responds to the combined thermal and mechanical disturbances. The spatial oscillations observed in the field distributions indicate the competing effects of wave propagation, attenuation, and coupling among the different physical mechanisms. Furthermore, the incorporation of conformable fractional derivatives introduces memory-dependent behavior, whereas Eringen's nonlocal elasticity accounts for microscale interactions. These features influence the propagation and attenuation characteristics of the coupled waves, making the response dependent not only on the electric-field intensity but also on the fractional and nonlocal parameters. Overall, Figure 6 highlights the importance of electric-field control in regulating the coupled photo-electro-thermoacoustic response of semiconductor materials. Such effects are relevant to the analysis and design of semiconductor devices subjected to combined electrical, thermal, and mechanical excitation. The results are consistent with the general framework of electromagnetic and thermoelastic coupling discussed in previous semiconductor studies [2,7,19,20,27]. The present model extends this framework by incorporating fractional-order dynamics and nonlocal elasticity into a unified photo-electro-magneto-thermoacoustic formulation.

Figure 7 presents the spatial distributions of the displacement components, temperature, normal stress, shear stress, carrier density, and acoustic pressure along the x-axis for different values of the phase-lag of the temperature gradient at $(\tau_\theta = 0)$, $(\tau_\theta = 0.04)$, and $(\tau_\theta = 0.29)$. The numerical results reveal that changes in the phase-lag of the temperature gradient affect the amplitudes, spatial variations, and attenuation characteristics of the physical fields. Depending on the field component, the response may exhibit enhanced or suppressed amplitudes, non-monotonic variations, or oscillatory behavior. These features demonstrate that the phase-lag of the temperature gradient plays an important role in determining the dynamic response of the coupled semiconductor system. From a physical perspective, the phase-lag of the temperature gradient characterizes the temporal response of the relevant transport or thermal process and determines how rapidly the system responds to an imposed disturbance. Changes in this parameter modify the phase relationship between the thermal, mechanical, and carrier-density fields, thereby influencing the propagation and attenuation of the associated waves. The resulting redistribution of thermal energy affects the temperature gradients and thermoelastic deformation, which subsequently modify the normal and shear stresses. Similarly, the carrier-density and acoustic-pressure distributions respond to the coupled evolution of charge carriers, thermal disturbances, and mechanical waves. The observed spatial variations can therefore be interpreted as a consequence of the competition between relaxation effects, wave propagation, and the interactions among the physical fields. In the present formulation, these mechanisms are further influenced by conformable fractional derivatives and Eringen's nonlocal elasticity theory. The fractional-order formulation accounts for memory-dependent behavior, while nonlocality incorporates the influence of microscale interactions on the mechanical response. Consequently, relaxation time provides an important parameter for controlling the attenuation and spatial distribution of coupled thermoelastic and photoacoustic waves in semiconductor media. These findings are consistent with the generalized thermoelastic frameworks of Lord and Shulman [13] and Green and Lindsay [14], as well as previous investigations of semiconductor wave propagation and fractional thermoelasticity [1,3,9,19,21]. The present study further examines the combined influence of relaxation effects, fractional-order dynamics, and nonlocal elasticity on the coupled electrical, thermal, mechanical, and acoustic responses.

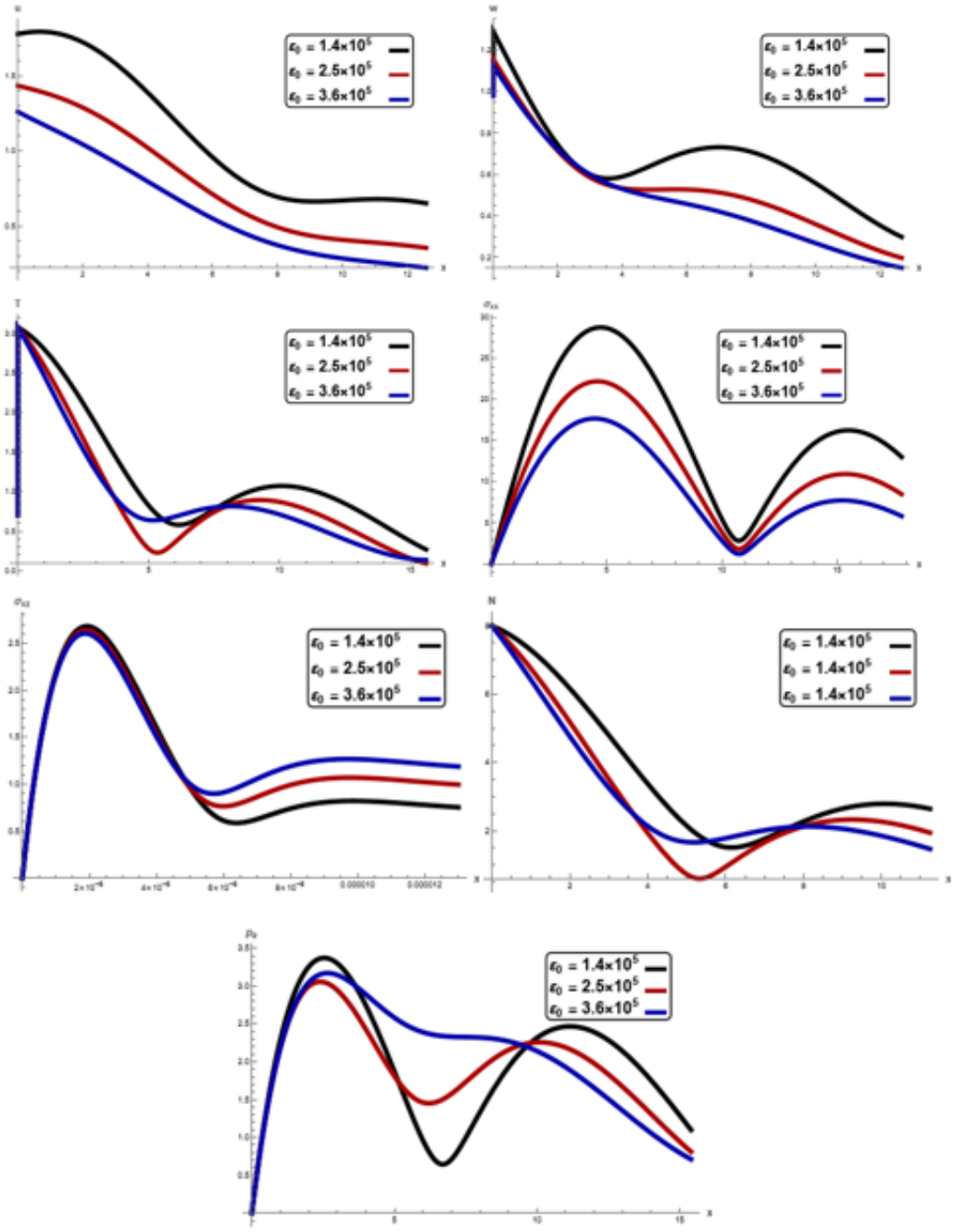


Figure 6. Effect of the electric field $(\boldsymbol{\varepsilon_0})$ on the evolution of the physical fields.

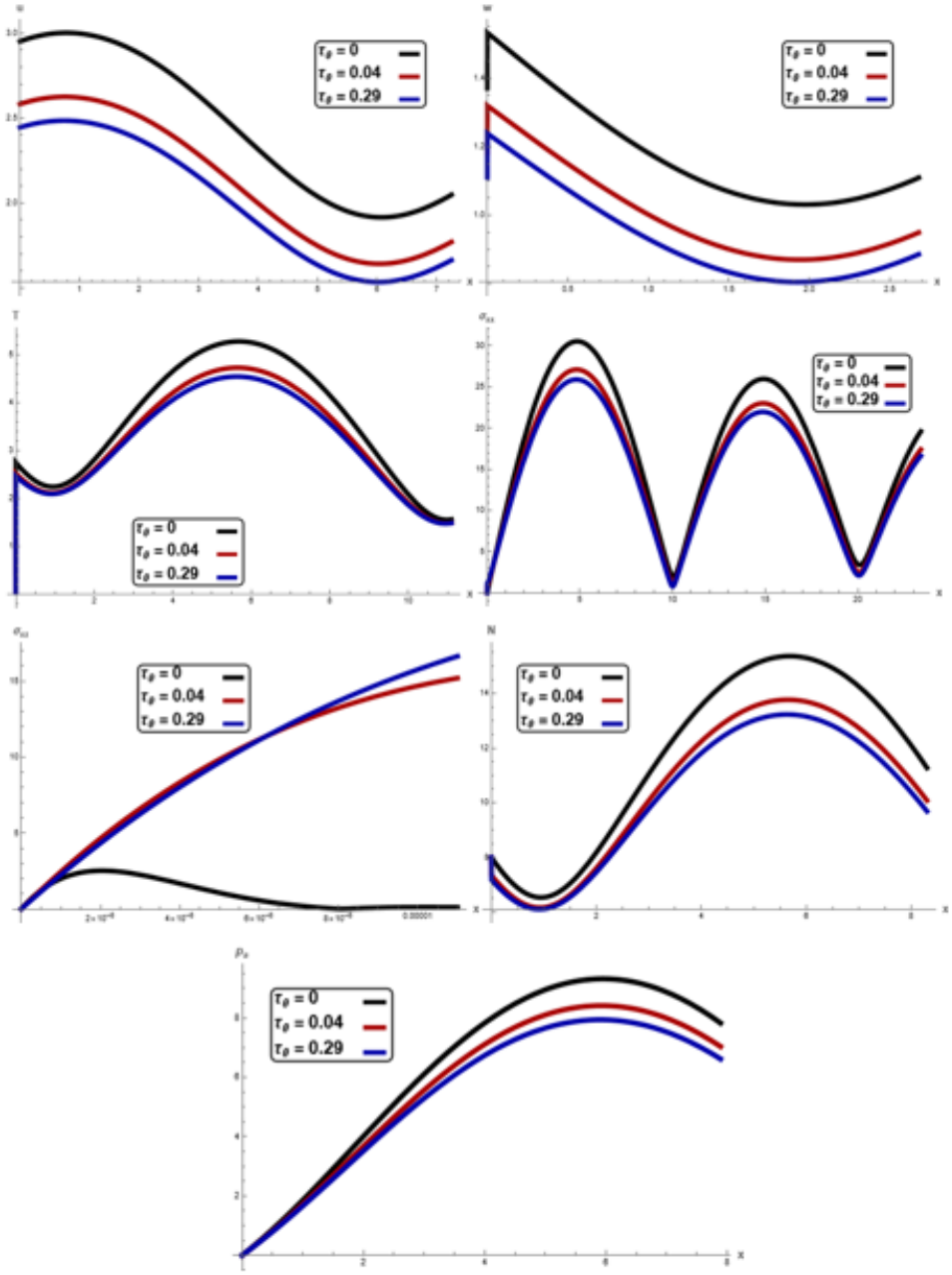


Figure 7. Effect of Relaxation time (τ_θ) on the evolution of the physical fields.

8. Conclusions

A comprehensive fractional-order model for photo-electro-magneto-thermoacoustic wave propagation in a nonlocal semiconductor medium has been developed, incorporating the effects of the initial stress, electric field, magnetic field, and relaxation time. The integration of conformable fractional derivatives with nonlocal elasticity theory enables accurate characterization of memory-dependent and microscale behaviors. The analytical treatment, based on normal-mode analysis, provides explicit insight into the coupled interactions among thermal, mechanical, electromagnetic, and carrier-density fields. Numerical investigations confirm that fractional parameters significantly influence wave attenuation and dispersion, while initial stress and

electromagnetic fields alter the stability and propagation characteristics. Furthermore, the wave propagation in the photo-thermoelastic variable exhibits clear sensitivity to the fractional order, magnetic field, and initial stress, indicating that photothermal mechanisms are strongly influenced by external forces. The present results are in good agreement with those reported in [35,37–39], confirming the validity of the proposed model. The proposed formulation offers a robust framework for analyzing multi-physical processes in semiconductors and can be extended to advanced applications in microelectronics and thermal engineering.

9. Future work

Future research may extend the present model by incorporating nonlinear thermoelastic effects and temperature-dependent material properties to enhance physical realism. The present fractional framework can also be generalized using alternative fractional operators such as Caputo–Fabrizio or Atangana–Baleanu derivatives to better describe complex memory effects. Moreover, extending the analysis to anisotropic or layered semiconductor structures would provide deeper insight into practical microelectronic applications. In the context of optical systems, the effect of the fractional-order derivative on the performance of neural network solutions for fractional differential equations can be studied. In addition, comparing the fractional conformable derivative with other fractional operators could provide deeper insight into photo-thermoelastic behavior. Experimental validation of the theoretical predictions under ultrafast laser excitation is also recommended to bridge the gap between theory and engineering applications.

Author contributions

Mashael A. Aljohani: Conceptualization, methodology, formulation of the research problem and solution approach; A. F. Al-Hazaemh: Analytical investigation, mathematical derivation, numerical computation, and visualization of the results; F. S. Bayones: Interpretation of the physical implications of the results and writing original draft preparation. All authors have read and approved the final version of the manuscript for publication.

Use of Generative-AI tools declaration

The authors declare that they have not used Artificial Intelligence (AI) tools in the creation of this article.

Acknowledgments

The authors would like to thank the Deanship of Graduate Studies and Scientific Research, Taif University, Saudi Arabia, for funding this work.

Funding

This work was funded by the Deanship of Graduate Studies and Scientific Research, Taif University.

Data availability

The data that support the findings of this study are available from the corresponding author upon reasonable request.

Conflicts of interest

The authors declare no conflicts of interest.

References

1. A. M. Alshehri, K. Lotfy, Dual-fractional photo-thermoacoustic modelling in rotating nonlocal semiconductor media with laser pulses, *Int. Commun. Heat Mass*, **172** (2026), 110312. https://doi.org/10.1016/j.icheatmasstransfer.2025.110312
2. K. K. Alarfaj, A. F. Al-Hazaemh, A. M. Abd-Alla, S. E. Abbas, Photo-electro-magneto-thermoelastic excitation rotating semiconductor medium based on focused laser beam, *Math. Sci.*, **20** (2026), 30–47. https://doi.org/10.57647/mathsci.2026.2001.02
3. H. H. Taha, A. H. El-Sharif, M. Adel, A. A. El-Bary, K. Lotfy, Fractional-order modeling of photo-thermoelastic waves in double-porosity semiconductor structures with decaying heat flux, *J. Low Freq. Noise V. A.*, **45** (2026), 226–243. https://doi.org/10.1177/14613484251380882
4. H. M. Alshehri, K. Lotfy, Fractional-order Hall-current magneto-photothermal waves in microtemperature hydro-poroelastic semiconductor media subjected to ramp-type heating and variable thermal conductivity, *Propuls. Power Res.*, **15** (2026), 276–299. https://doi.org/10.1016/j.jppr.2026.03.002
5. A. Kamel, N. A. Yaseen, A. A. El-Bary, W. S. Hassanin, K. Lotfy, Photo-thermoacoustic waves propagation flow of excited magneto-nonlocal semiconductors in stability region with varying thermal conductivity, *Phys. Fluids*, **36** (2024), 087139. https://doi.org/10.1063/5.0215514
6. A. Ahlawat, S. Chaudhary, A. Kumar, K. Ghachem, A. Mir, L. Kolsi, Photo-thermo-acoustic interactions in a fiber-reinforced nonlocal semiconductor medium, *Int. J. Numer. Method. H.*, **36** (2026), 2142–2167. https://doi.org/10.1108/HFF-12-2025-0975
7. A. Sur, Photothermoelastic interaction in a two-dimensional semiconductor with nonlocal stress theory, *Int. J. Comput. Meth. En.*, **25** (2024), 248–264. https://doi.org/10.1080/15502287.2024.2338548
8. I. Kaur, K. Singh, Plane wave in non-local semiconducting rotating media with Hall effect and three-phase lag fractional order heat transfer, *Int. J. Mech. Mater. Eng.*, **16** (2021), 14. https://doi.org/10.1186/s40712-021-00137-3
9. K. Lotfy, I. S. Elshazly, I. Bachar, S. Sharma, A. A. El-Bary, N. A. Yaseen, Fractional photo-thermoelastic waves of hydrodynamic semiconductors with Hall currents and variable thermal conductivity, *Case Stud. Therm. Eng.*, **71** (2025), 106180. https://doi.org/10.1016/j.csite.2025.106180
10. S. El-Sapa, W. Alhejail, K. Lotfy, A. A. El-Bary, Excited non-local microelongated semiconductor layer thermal-optical mechanical waves affected by rotational field, *Crystals*, **13** (2023), 116. https://doi.org/10.3390/cryst13010116

11. A. Kamel, S. El-Sapa, A. A. El-Bary, K. Lotfy, Novel multi-temperature photoacoustic dynamics in nanoscale hydro-semiconductors under variable thermal conductivity, *Sci. Rep.*, **15** (2025), 26710. https://doi.org/10.1038/s41598-025-12756-3
12. M. A. Biot, Thermoelasticity and irreversible thermodynamics, *J. Appl. Phys.*, **27** (1956), 240–253. https://doi.org/10.1063/1.1722351
13. H. W. Lord, Y. Shulman, A generalized dynamical theory of thermoelasticity, *J. Mech. Phys. Solids*, **15** (1967), 299–309. https://doi.org/10.1016/0022-5096(67)90024-5
14. A. E. Green, K. A. Lindsay, Thermoelasticity, *J. Elasticity*, **2** (1972), 1–7. https://doi.org/10.1007/BF00045689
15. R. M. White, Generation of elastic waves by transient surface heating, *J. Appl. Phys.*, **34** (1963), 3559–3567. https://doi.org/10.1063/1.1729258
16. K. Lotfy, Photothermal waves for two temperature with a semiconducting medium under using a dual-phase-lag model and hydrostatic initial stress, *Wave. Random Complex*, **27** (2017), 482–501. https://doi.org/10.1080/17455030.2016.1267416
17. M. Adel, S. El-Sapa, A. A. El-Bary, K. Lotfy, E. Can, Photoacoustic wave dynamics in magneto-hydro-semiconductor media with rotation and multi-temperature effects, *Case Stud. Therm. Eng.*, **72** (2025), 106432. https://doi.org/10.1016/j.csite.2025.106432
18. M. H. Raddadi, A. El-Bary, R. S. Tantawi, N. Anwer, K. Lotfy, A novel model of semiconductor porosity medium according to photo-thermoelasticity excitation with initial stress, *Crystals*, **12** (2022), 1603. https://doi.org/10.3390/cryst12111603
19. D. M. Salah, A. M. Abd-Alla, S. M. Abo-Dahab, A. M. Alharbi, M. A. Abdelhafez, Magneto-thermoelastic semiconductor medium with diffusion under the hyperbolic two-temperature photothermal waves, *Mech. Solids*, **59** (2024), 1774–1791. https://doi.org/10.1134/S0025654424603768
20. A. F. Al-Hazaemh, A. M. Abd-Alla, S. E. Abbas, Photothermal interactions in micropolar generalized thermoelastic medium subjected to electromagnetic field, *Sci. Rep.*, **15** (2025), 39576. https://doi.org/10.1038/s41598-025-23882-3
21. G. M. Ismail, K. A. Gepreel, Kh. Lotfy, A. M. S. Mahdy, A. El-Bary, A. M. Saeed, Influence of variable thermal conductivity on thermal-plasma-elastic waves of excited microelongated semiconductor, *Alex. Eng. J.*, **61** (2022), 12271–12282. https://doi.org/10.1016/j.aej.2022.06.024
22. K. Lotfy, W. Hassan, Normal mode method for two-temperature generalized thermoelasticity under thermal shock problem, *J. Therm. Stresses*, **37** (2014), 545–560. https://doi.org/10.1080/01495739.2013.869145
23. M. I. A. Othman, K. Lotfy, Effect of rotation on plane waves in generalized thermo-microstretch elastic solid with one relaxation time, *Multidiscipl. Model. Ma.*, **7** (2011), 43–62. https://doi.org/10.1108/15736101111141430
24. S. El-Sapa, A. A. Almoneef, K. Lotfy, A. A. El-Bary, A. M. Saeed, Moore-Gibson-Thompson theory of a non-local excited semiconductor medium with stability studies, *Alex. Eng. J.*, **61** (2022), 11753–11764. https://doi.org/10.1016/j.aej.2022.05.036
25. M. C. Zhao, O. Nikan, An L2-type time-discrete method for mixed fractional Sobolev-type equations on general nonuniform meshes, *Numer. Algor.*, in press. https://doi.org/10.1007/s11075-026-02327-6

26. O. Nikan, J. Rashidinia, H. Jafari, An improved local radial basis function method for pricing options under the time-fractional Black–Scholes model, *J. Comput. Sci.*, **89** (2025), 102610. https://doi.org/10.1016/j.jocs.2025.102610
27. X. Wang, K. Dong, Magneto-thermo-dynamic stress and perturbation of magnetic field vector in a non-homogeneous thermo-elastic cylinder, *Eur. J. Mech. A-Solid.*, **25** (2006), 98–109. https://doi.org/10.1016/j.euromechsol.2005.07.003
28. A. M. Abd-Alla, S. E. Abbas, A. F. Al-Hazaemh, Thermal stress in an elastic half-space and its application in partial differential equation, *Mech. Solids*, **60** (2025), 3661–3670. https://doi.org/10.1134/S0025654425600655
29. M. Soliman, H. M. Ahmed, N. Badra, T. A. Nofal, I. Samir, Highly dispersive gap solitons for conformable fractional model in optical fibers with dispersive reflectivity solutions using the modified extended direct algebraic method, *AIMS Math.*, **9** (2024), 25205–25222. https://doi.org/10.3934/math.20241229
30. D. Z. Zhao, M. K. Luo, General conformable fractional derivative and its physical interpretation, *Calcolo*, **54** (2017), 903–917. https://doi.org/10.1007/s10092-017-0213-8
31. A. C. Eringen, A continuum theory of superconductivity, *Z. Angew. Math. Phys.*, **53** (2002), 1026–1037. https://doi.org/10.1007/PL00013844
32. K. K. Alarfaj, A. F. Al-Hazaemh, A. M. Abd-Alla, Ramp-type heating in a thermoelastic semiconductor medium under coupled plasma and thermal with gravity and initial stress effects, *Propuls. Power Res.*, **15** (2026), 537–550. https://doi.org/10.1016/j.jppr.2026.05.004
33. X. L. Qi, C. S. Suh, Generalized thermo-elastodynamics for semiconductor material subject to ultrafast laser heating. Part I: Model description and validation, *Int. J. Heat Mass Tran.*, **53** (2010), 41–47. https://doi.org/10.1016/j.ijheatmasstransfer.2009.10.010
34. D. K. Markushev, D. D. Markushev, S. M. Aleksić, D. S. Pantić, S. P. Galović, D. M. Todorović, et al., Experimental photoacoustic observation of the photogenerated excess carrier influence on the thermoelastic response of n-type silicon, *J. Appl. Phys.*, **128** (2020), 095103. https://doi.org/10.1063/5.0015657
35. A. Ramady, M. F. Ismail, H. M. Ahmed, S. Alkhatib, E. M. Ramadan, E. N. S. El-Ganzoury, Effect of rotation on wave propagation in micro-elongated thermo-elastic media with fractional conformable derivative under the refined dual-phase-lag model, *Math. Sci.*, **20** (2026), 1–11. https://doi.org/10.57647/mathsci.2026.46781
36. R. Javadi, H. Mesgarani, O. Nikan, Z. Avazzadeh, Solving fractional order differential equations by using fractional radial basis function neural network, *Symmetry*, **15** (2023), 1275. https://doi.org/10.3390/sym15061275
37. W. L. Qiu, O. Nikan, Z. Avazzadeh, Numerical investigation of generalized tempered-type integrodifferential equations with respect to another function, *Fract. Calc. Appl. Anal.*, **26** (2023), 2580–2601. https://doi.org/10.1007/s13540-023-00198-5
38. A. Ramady, M. F. Ismail, H. M. Ahmed, S. Alkhatib, M. E. Ramadan, E. N. S. El-Ganzoury, The effects of fractional derivative and gravity on wave propagation in micro-elongated thermo-elastic media under the refined dual-phase-lag model, *Sci. Rep.*, **16** (2026), 3454. https://doi.org/10.1038/s41598-025-33427-3

39. M. E. Ramadan, H. M. Ahmed, T. Radwan, Y. Yildirim, H. Elsadek, M. F. Ismail, Initial stress effects on fractional thermoelastic wave propagation in semiconductor media under three thermoelasticity theories, *Sci. Progress*, **109** (2026), 1–16. https://doi.org/10.1177/00368504261467847
40. R. F. Zhang, Z. L. Zhao, Y. F. Hu, J. H. Kang, Neural-symbolic exact solutions for Camassa–Holm equation, *Neurocomputing*, **706** (2026), 135040. https://doi.org/10.1016/j.neucom.2026.135040
41. Z. L. Zhao, R. F. Zhang, Artificial intelligence-enhanced mathematical derivation method: Exact solutions of the Benjamin–Bona–Mahony equation, *Eng. Appl. Artif. Intel.*, **173** (2026), 114464. https://doi.org/10.1016/j.engappai.2026.114464
42. H. W. Zhang, R. F. Zhang, Q. R. Liu, A novel multi-modal neurosymbolic reasoning intelligent algorithm for BLMP equation, *Chinese Phys. Lett.*, **42** (2025), 100002. https://doi.org/10.1088/0256-307X/42/10/100002
43. L. Meng, X. R. Zhang, L. F. Lin, S. H. Shi, H. Q. Wang, Collective dynamics of fractional oscillators with fluctuating frequency in Erdős–Rényi random networks, *Commun. Nonlinear Sci.*, **159** (2026), 109919. https://doi.org/10.1016/j.cnsns.2026.109919
44. R. Q. Zhang, X. J. Zhu, L. F. Lin, S. H. Shi, H. Q. Wang, Collective dynamical behaviors of coupled Langevin oscillators with damping fluctuation in attractive–repulsive weighted random networks, *Physica A*, **689** (2026), 131431. https://doi.org/10.1016/j.physa.2026.131431

Appendix A

The coefficients are defined as follows:

$$S_{11} = K_{12} / K_{11}$$

$$S_{12} = K_{13} / K_{11}$$

$$S_{13} = K_{14} / K_{11}$$

$$S_{14} = K_{15} / K_{11}$$

$$S_{15} = K_{16} / K_{11}$$

$$K_{11} = \beta_{12}\,\beta_5\,\beta_7\,\varepsilon_{13}$$

$$\begin{aligned} K_{12} = {} & (\beta_{12}\,\beta_5\,\beta_7\,\beta_9 + \beta_{12}\,\beta_2\,\beta_4\,\beta_7\,\varepsilon_{13} + b^2\,\beta_{12}\,\beta_5\,\beta_7\,\varepsilon_{13} + \beta_1\,\beta_{12}\,\beta_5\,\beta_7\,\varepsilon_{13} + \beta_{13}\,\beta_5\,\beta_7\,\varepsilon_{13} \\ & + \beta_{12}\,\beta_6\,\beta_7\,\varepsilon_{13} - \beta_{12}\,\beta_5\,\beta_8\,\varepsilon_{13} - \beta_{12}\,\beta_7\,\delta_{12}\,\varepsilon_{13} - \beta_{11}\,\beta_5\,\beta_7\,\varepsilon_{13}\,\varepsilon_3) \end{aligned}$$

$$\begin{aligned} K_{13} = {} & (-\beta_{12}\,\beta_2\,\beta_4\,\beta_7\,\beta_9 - b^2\,\beta_{12}\,\beta_5\,\beta_7\,\beta_9 - \beta_1\,\beta_{12}\,\beta_5\,\beta_7\,\beta_9 - \beta_{13}\,\beta_5\,\beta_7\,\beta_9 - \beta_{12}\,\beta_6\,\beta_7\,\beta_9 \\ & + \beta_{12}\,\beta_5\,\beta_8\,\beta_9 + \beta_{12}\,\beta_7\,\beta_9\,\delta_{12} - b^2\,\beta_{12}\,\beta_2\,\beta_4\,\beta_7\,\varepsilon_{13} - \beta_{13}\,\beta_2\,\beta_4\,\beta_7\,\varepsilon_{13} - b^2\,\beta_1\,\beta_{12}\,\beta_5\,\beta_7\,\varepsilon_{13} \\ & - \beta_1\,\beta_{13}\,\beta_5\,\beta_7\,\varepsilon_{13} - b^2\,\beta_{12}\,\beta_6\,\beta_7\,\varepsilon_{13} - \beta_1\,\beta_{12}\,\beta_6\,\beta_7\,\varepsilon_{13} - \beta_{13}\,\beta_6\,\beta_7\,\varepsilon_{13} + \beta_{12}\,\beta_2\,\beta_4\,\beta_8\,\varepsilon_{13} \\ & + b^2\,\beta_{12}\,\beta_5\,\beta_8\,\varepsilon_{13} + \beta_1\,\beta_{12}\,\beta_5\,\beta_8\,\varepsilon_{13} + \beta_{13}\,\beta_5\,\beta_8\,\varepsilon_{13} + \beta_{12}\,\beta_6\,\beta_8\,\varepsilon_{13} + b^2\,\beta_{12}\,\beta_7\,\delta_{12}\,\varepsilon_{13} \\ & + \beta_{13}\,\beta_7\,\delta_{12}\,\varepsilon_{13} - \beta_{12}\,\beta_8\,\delta_{12}\,\varepsilon_{13} + \beta_5\,\varepsilon_{12}\,\varepsilon_{13}\,\varepsilon_{18} + \beta_{11}\,\beta_5\,\beta_7\,\beta_9\,\varepsilon_3 + i\,b\,\beta_{11}\,\beta_4\,\beta_7\,\varepsilon_{13}\,\varepsilon_3 \\ & + b^2\,\beta_{11}\,\beta_5\,\beta_7\,\varepsilon_{13}\,\varepsilon_3 + \beta_{11}\,\beta_6\,\beta_7\,\varepsilon_{13}\,\varepsilon_3 - \beta_{11}\,\beta_5\,\beta_8\,\varepsilon_{13}\,\varepsilon_3 - \beta_{11}\,\beta_5\,\varepsilon_{12}\,\varepsilon_{13}\,\varepsilon_3) \end{aligned}$$

$$K_{14} = (b^2 \beta_{12} \beta_2 \beta_4 \beta_7 \beta_9 + \beta_{13} \beta_2 \beta_4 \beta_7 \beta_9 + b^2 \beta_1 \beta_{12} \beta_5 \beta_7 \beta_9 + \beta_1 \beta_{13} \beta_5 \beta_7 \beta_9 + b^2 \beta_{12} \beta_6 \beta_7 \beta_9 + \beta_1 \beta_{12} \beta_6 \beta_7 \beta_9 + \beta_{13} \beta_6 \beta_7 \beta_9 - \beta_{12} \beta_2 \beta_4 \beta_8 \beta_9 - b^2 \beta_{12} \beta_5 \beta_8 \beta_9 - \beta_1 \beta_{12} \beta_5 \beta_8 \beta_9 - \beta_{13} \beta_5 \beta_8 \beta_9 - \beta_{12} \beta_6 \beta_8 \beta_9 - b^2 \beta_{12} \beta_7 \beta_9 \delta_{12} - \beta_{13} \beta_7 \beta_9 \delta_{12} + \beta_{12} \beta_8 \beta_9 \delta_{12} + b^2 \beta_1 \beta_{12} \beta_6 \beta_7 \varepsilon_{13} + \beta_1 \beta_{13} \beta_6 \beta_7 \varepsilon_{13} - b^2 \beta_{12} \beta_2 \beta_4 \beta_8 \varepsilon_{13} - \beta_{13} \beta_2 \beta_4 \beta_8 \varepsilon_{13} - b^2 \beta_1 \beta_{12} \beta_5 \beta_8 \varepsilon_{13} - \beta_1 \beta_{13} \beta_5 \beta_8 \varepsilon_{13} - b^2 \beta_{12} \beta_6 \beta_8 \varepsilon_{13} - \beta_1 \beta_{12} \beta_6 \beta_8 \varepsilon_{13} - \beta_{13} \beta_6 \beta_8 \varepsilon_{13} + b^2 \beta_{12} \beta_8 \delta_{12} \varepsilon_{13} + \beta_{13} \beta_8 \delta_{12} \varepsilon_{13} - \beta_5 \beta_9 \varepsilon_{12} \varepsilon_{18} - \beta_2 \beta_4 \varepsilon_{12} \varepsilon_{13} \varepsilon_{18} - \beta_1 \beta_5 \varepsilon_{12} \varepsilon_{13} \varepsilon_{18} - \beta_6 \varepsilon_{12} \varepsilon_{13} \varepsilon_{18} + \delta_{12} \varepsilon_{12} \varepsilon_{13} \varepsilon_{18} - i\, b \beta_{11} \beta_4 \beta_7 \beta_9 \varepsilon_3 - b^2 \beta_{11} \beta_5 \beta_7 \beta_9 \varepsilon_3 - \beta_{11} \beta_6 \beta_7 \beta_9 \varepsilon_3 + \beta_{11} \beta_5 \beta_8 \beta_9 \varepsilon_3 + \beta_{11} \beta_5 \beta_9 \varepsilon_{12} \varepsilon_3 - b^2 \beta_{11} \beta_6 \beta_7 \varepsilon_{13} \varepsilon_3 + i\, b \beta_{11} \beta_4 \beta_8 \varepsilon_{13} \varepsilon_3 + b^2 \beta_{11} \beta_5 \beta_8 \varepsilon_{13} \varepsilon_3 + \beta_{11} \beta_6 \beta_8 \varepsilon_{13} \varepsilon_3 + i\, b \beta_{11} \beta_4 \varepsilon_{12} \varepsilon_{13} \varepsilon_3 + b^2 \beta_{11} \beta_5 \varepsilon_{12} \varepsilon_{13} \varepsilon_3 + \beta_{11} \beta_6 \varepsilon_{12} \varepsilon_{13} \varepsilon_3)$$

$$K_{15} = (-b^2 \beta_1 \beta_{12} \beta_6 \beta_7 \beta_9 - \beta_1 \beta_{13} \beta_6 \beta_7 \beta_9 + b^2 \beta_{12} \beta_2 \beta_4 \beta_8 \beta_9 + \beta_{13} \beta_2 \beta_4 \beta_8 \beta_9 + b^2 \beta_1 \beta_{12} \beta_5 \beta_8 \beta_9 + \beta_1 \beta_{13} \beta_5 \beta_8 \beta_9 + b^2 \beta_{12} \beta_6 \beta_8 \beta_9 + \beta_1 \beta_{12} \beta_6 \beta_8 \beta_9 + \beta_{13} \beta_6 \beta_8 \beta_9 - b^2 \beta_{12} \beta_8 \beta_9 \delta_{12} - \beta_{13} \beta_8 \beta_9 \delta_{12} + b^2 \beta_1 \beta_{12} \beta_6 \beta_8 \varepsilon_{13} + \beta_1 \beta_{13} \beta_6 \beta_8 \varepsilon_{13} + \beta_2 \beta_4 \beta_9 \varepsilon_{12} \varepsilon_{18} + \beta_1 \beta_5 \beta_9 \varepsilon_{12} \varepsilon_{18} + \beta_6 \beta_9 \varepsilon_{12} \varepsilon_{18} - \beta_9 \delta_{12} \varepsilon_{12} \varepsilon_{18} + \beta_1 \beta_6 \varepsilon_{12} \varepsilon_{13} \varepsilon_{18} + b^2 \beta_{11} \beta_6 \beta_7 \beta_9 \varepsilon_3 - i\, b \beta_{11} \beta_4 \beta_8 \beta_9 \varepsilon_3 - b^2 \beta_{11} \beta_5 \beta_8 \beta_9 \varepsilon_3 - \beta_{11} \beta_6 \beta_8 \beta_9 \varepsilon_3 - i\, b \beta_{11} \beta_4 \beta_9 \varepsilon_{12} \varepsilon_3 - b^2 \beta_{11} \beta_5 \beta_9 \varepsilon_{12} \varepsilon_3 - \beta_{11} \beta_6 \beta_9 \varepsilon_{12} \varepsilon_3 - b^2 \beta_{11} \beta_6 \beta_8 \varepsilon_{13} \varepsilon_3 - b^2 \beta_{11} \beta_6 \varepsilon_{12} \varepsilon_{13} \varepsilon_3)$$

$$K_{16} = (b^2 \beta_1 \beta_{12} \beta_6 \beta_8 \beta_9 + \beta_1 \beta_{13} \beta_6 \beta_8 \beta_9 + \beta_1 \beta_6 \beta_9 \varepsilon_{12} \varepsilon_{18} - b^2 \beta_{11} \beta_6 \beta_8 \beta_9 \varepsilon_3 - b^2 \beta_{11} \beta_6 \beta_9 \varepsilon_{12} \varepsilon_3).$$

AIMS Press

© 2026 the Author(s), licensee AIMS Press. This is an open access article distributed under the terms of the Creative Commons Attribution License (https://creativecommons.org/licenses/by/4.0)